Table SI. *Titres of antibody against herpes viruses during the course treatment with intravenous immunoglobulin*

| Day* | | | –4 | 3 | 17 | 31 | 59 |
|---|---|---|---|---|---|---|---|
| HHV-6** | IgG | | 320 | 640 | 160 | 320 | 640 |
| | IgM | | <10 | <10 | <10 | <10 | <10 |
| CMV** | IgG | | ND | 53.0 | 32.6 | 32.0 | 34.9 |
| | IgM | | ND | 0.46 | 0.16 | 0.43 | 0.50 |
| EBV** | VCA | IgG | ND | 160 | 160 | 160 | 160 |
| | | IgM | ND | <10 | <10 | <10 | <10 |
| | EADR | IgG | ND | <10 | <10 | <10 | <10 |
| | NA | IgG | ND | 80 | 80 | 80 | 80 |

*Number indicates time (days) after the eruption. The time-point when the eruption initiated was designated day 0. Virus titre of the preserved serum is also indicated in the first column at day –4. **Titres of antibody against HHV-6/EBV and CMV were measured by fluorescent antibody method and enzyme immunoassay (negative, <1.0), respectively.
VCA: virus capsid antigen; EADR: early antigen-diffuse and restrict complex; NA: nuclear antigen. ND: not done. IVIG therapy was started from day 3 for successive 5 days.

# Rosacea-like Demodicosis Mimicking Cutaneous Lymphoma

**Yukiko Kito, Hideo Hashizume and Yoshiki Tokura**
*Department of Dermatology, Hamamatsu University School of Medicine, 1-20-1 Handayama, Higashi-ku, Hamamatsu 431-3192, Japan. E-mail: yukikok@hama-med.ac.jp*
*Accepted May 31, 2011.*

Demodex mites may play a pathogenic role when present in excessive numbers or when penetrating into the dermis. There are two types of mites. *Demodex folliculorum* is usually found in the follicular infundibulum, and *D. brevis* in sebaceous ducts and meibomian glands (1, 2). Pityriasis folliculorum is one of the typical skin manifestations of Demodex, and is characterized by facial erythema with follicular plugs and scale producing a "nutmeg-grater" or "sandpaper-like" appearance. Histologically, the eruption exhibits perivascular and diffuse dermal infiltration of lymphocytes without granuloma formation.

Rosacea-like demodicosis is another representative eruption characterized by follicular scaling, sudden onset, rapid progression, and no history of flushing (3, 4). In addition, meibomian gland dysfunction and keratoconjunctivitis may occur as eye lesions (5). Notably, there may be eyelid involvement, called demodectic blepharitis. Biopsies show a primary perifollicular infiltrate of mononuclear cells, with possible granulomatous inflammation. Demodicosis gravis represents a more severe form of demodicosis and shows intriguing granulomatous rosacea. Biopsies show granulomas with central caseation necrosis and foreign-body-type multinucleated giant cell (3, 4).

We report here two patients with rosacea-like demodicosis who had indurated lesions with massive lymphocytic infiltrates on the eyelids, forehead and cheeks and congestion of the eyes.

## CASE REPORTS

### *Case 1*

A 55-year-old healthy man had a one-year history of pruritic skin eruption on the face, which was treated with corticosteroid ointment without therapeutic effect. Subsequently, he developed blepharoedema and sclera-oedema on the left cheek, acne-rosacea-like rash with red papules and telangiectasia on his lower jaw, and congestion on his left eye. On examination, the patient had sclera-oedematous lesions on the left eyelids, left upper cheek and two subcutaneous nodules around his glabella (Fig. 1a). A skin biopsy specimen from the cheek showed a dense lymphocytic infiltrate around hair follicles (Fig. 2a). In serial sections, multiple Demodex mites were packed inside the infundibulum and sebaceous glands. The lymphocytes were positive for CD3, CD4, and partially CD8, and negative for CD20, CD30, CD56, CD79a, TIA-1, granzyme B and Epstein-Barr virus (EBV)-encoded RNA (EBER). Although the infiltrate consisted of small lymphoid cells without atypia, oligoclonal pattern of T-cell receptor (TCR) gene rearrangement was detected in the biopsy specimen by a PCR-based detection method. In another specimen from a subcutaneous nodule on the forehead, there was sarcoidal granuloma, with Langhans and foreign-body-type multinucleated giant cells in the dermis and subcutaneous tissue (Fig. 2b). Periodic acid-Schiff (PAS), Grocott and Ziehl-Neelsen stains were negative.

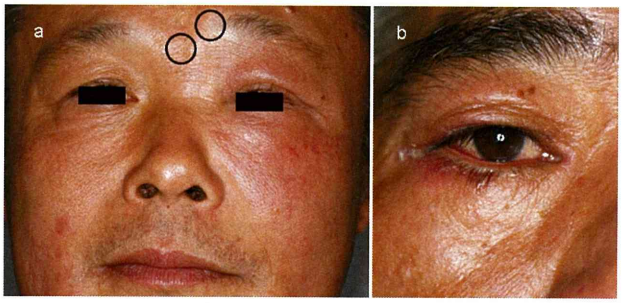


*Fig. 1.* (a) Blepharoedema and sclera-oedema on the left aspect of the face and two subcutaneous nodules around the glabella (*circles*) (case 1). (b) Sclero-oedema of the nose, erythema on the inferior eyelid, and congestion on the right eye (case 2).

Laboratory investigations revealed normal blood chemistry, including serum glucose and angiotensin-converting enzyme, and humoral and cellular immunity. Soluble IL-2 receptor level was normal, and thymidine kinase activity was slightly elevated (8.5; normal < 5 U/l). Titres of antibodies against EBV and human immunodeficiency virus (HIV), and copies of EBV were unremarkable. Magnetic resonance imaging of the

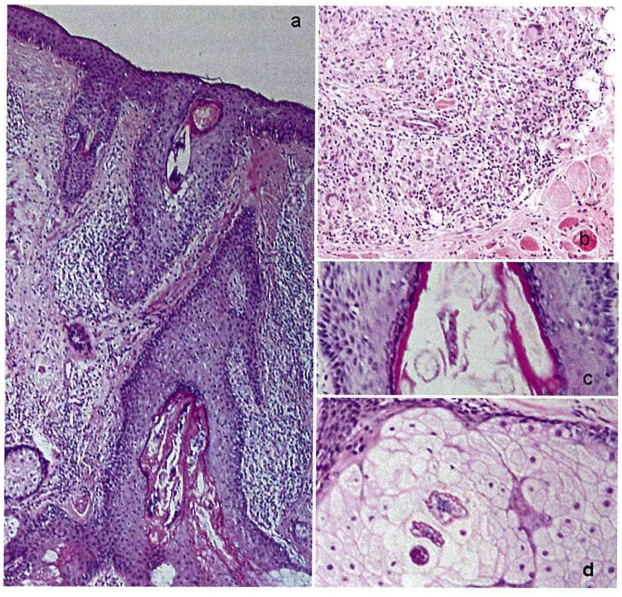


*Fig. 2.* (a) In a specimen from the cheek, there is a dense perifollicular lymphocytic infiltrate and multiple Demodex mites are present inside the infundibulum. (b) In a specimen from the glabella, there is sarcoidal granuloma consisting of Langhans and foreign-body-type multinucleated giant cells (case 1). (c) In a specimen from the nose, Demodex mites are present inside the hair follicles. (d) Demodex in sebaceous glands (case 2).

 doi: 10.2340/00015555-1200
 ISSN 0001-5555

head revealed hypertrophy of subcutaneous tissue around his left eyelid and cheek, but no abnormalities in the nasal cavity, paranasal sinus or orbit. Chest and abdominal CT disclosed neither lymphadenopathy nor pulmonary involvement. We thus ruled out tuberculoid sarcoidosis and leprosy. The patient was treated with oral ivermectin and topical crotamiton, which markedly improved blepharoedema and facial sclera-oedema and subcutaneous nodules. We again performed skin biopsy from his cheek, and there was a slight perifollicular infiltrate without granuloma. No TCR gene rearrangement was detected in the specimen, suggesting that Demodex mites played a pathogenic role for the monoclonal infiltration of T cells.

*Case 2*

A 64-year-old healthy man presented with a 6-month history of indurations on the nose and right cheek. He also had erythema on his inferior eyelid margin, with scaling at the root of eyelash and congestion on his right eye (Fig. 1b). No lymphadenopathy was found. Laboratory investigations revealed no humoral or cellular immunodeficiency, and no elevation of antibodies against EBV antigens. Skin biopsy from his nose showed a dense perifollicular lymphocytic infiltrate and the presence of Demodex mites inside hair follicles (Fig. 2c) and sebaceous glands (Fig. 2d). TCR gene rearrangement was not present in the biopsy specimen. The patient was treated with oral minocycline, and sclerosis of the nose, blepharitis and congestion on his right eye disappeared dramatically.

## DISCUSSION

In the two patients with demodicosis, rosacea-like eruptions, blepharitis and conjunctivitis are the known lesions caused by Demodex. Demodex blepharitis is often misdiagnosed as other corneal and external diseases, and should be kept in mind on seeing refractory blepharitis, conjunctivitis and keratitis in adult patients or blepharoconjunctivitis and recurrent chalazia in young patients (5). Massive infiltration of lymphocytes and monoclonal expansion of T cells was a novel finding in our patients. It is known that the pathogenic mechanisms of demodicosis include sequential occurrence of the following events: (*i*) occlusion of hair follicles and sebaceous ducts by the mites or possible reactive hyperkeratosis; (*ii*) host's cell-mediated immune reactions by the mites or their waste products; (*iii*) further foreign body granulomatous reaction to the chitinous skeleton of mites; and (*iv*) possible modulation by a vector role for bacteria (3). Superantigens produced by *Staphylococci* and *Streptococci* are also implicated in the induction of rosacea (6).

Demodex may feed on follicular and glandular epithelial cells, leading to direct damage of the lid. *D. folliculorum* has been reported to consume epithelial cells at the hair follicle, which results in follicular distension, and subsequent formation of loose or misdirected lashes. The resultant trichiasis may induce trauma to the corneal epithelium (5). On the other hand, *D. brevis* can mechanically block the orifices of meibomian glands, giving rise to meibomian gland dysfunction with lipid tear deficiency (7), and ophthalmologically, *D. brevis* increases evaporation of tears and causes keratoconjunctivitis. *D. brevis* usually burrows deep into the sebaceous and meibomian glands, and its chitinous exoskeleton may act as a foreign body causing granulomatous reaction, which causes recurrent and refractory chalazia (8, 9).

In the two cases described here, facial sclera-oedema and blepharoedema with histological massive lymphocytic infiltration mimicked cutaneous lymphoma. The treatment of Demodex was therapeutically effective for the congestion of the eyes as well as the skin lesions in both cases. The disappearance of monoclonality of T cells may provide evidence for stimulation of certain populations of T cells with mite antigen. The cases described here suggest that rosacea-like demodicosis occasionally resembles cutaneous lymphoma, and the eye lesions may be informative for suspecting demodicosis.

*The authors declare no conflicts of interest.*

## REFERENCES

1. Ecker RI, Winkelmann RK. Demodex granuloma. Arch Dermatol 1979; 115: 343–344.
2. Hoekzema R, Hulsevosch HJ, Bos JD. Demodecosis or rosacea: what did we treat? Br J Dermatol 1995; 133: 294–299.
3. Baima B, Sticherling M. Demodicidosis revisited. Acta Derm Venereol 2002; 82: 3–6.
4. De Dulanto F, Camacho-Martinesz F. Demodicosis gravis Ann Dermatol Venerol 1979; 106: 699–704.
5. Liu J, Sheha H, Tseng SC. Pathogenic role of Demodex mites in blepharitis. Curr Opin Allergy Clin Immunol 2010; 10: 505–510.
6. Wolf R, Ophir J, Avigad J, Lengy J, Krakowski A. The hair follicle mites (Demodex spp.) Could they be vectors of pathogenic microorganisms? Acta Derm Venereol 1988; 68: 535–537.
7. Gao YY, Di Pascuale MA, Elizondo A, Tseng SC. Clinical treatment of ocular demodecosis by lid scrub with tea tree oil. Cornea 2007; 26: 136–143.
8. English FP, Cohn D, Groeneveld ER. Demodectic mites and chalazion. Am J Ophthalmol 1985; 100: 482–483.
9. Koksal M, Kargi S, Taysi BN, Ugurbas SH. A rare agent of chalazion: demodectic mites. Can J Ophthalmol 2003; 38: 605–606.

# Epstein-Barr Virus-positive Mucocutaneous Ulcers as a Manifestation of Methotrexate-associated B-cell Lymphoproliferative Disorders

**Hideo Hashizume[1], Izumi Uchiyama[2], Tetsuya Kawamura[3], Takafumi Suda[4], Masahiro Takigawa[2] and Yoshiki Tokura[2]**

*[1]Divison of Dermatology, Shimada Municipal Hospital, 1200-5 Noda, Shimada 427-8502, [2]Department of Dermatology, Hamamatsu University School of Medicine, Hamamatsu, [3]Division of Dermatology, Numazu City Hospital, Numazu, and [4]Second Division, Department of Internal Medicine, Hamamatsu University School of Medicine, Hamamatsu, Japan. E-mail: hihashiz@hama-med.ac.jp*

*Accepted September 20, 2011.*

Immunosuppressive states due to immunological senescence (1) or administration of immunosuppressants (2) occasionally cause Epstein-Barr virus (EBV)-induced B-cell lymphoproliferative disorders (LPDs). While methotrexate (MTX) is an anti-metabolite and anti-foliate agent for the treatment of cancers and autoimmune disorders, it can also potentiate tumourigenesis due to its immunosuppressive effect. EBV reactivation is observed in half of such cases, suggesting that EBV contributes to the pathogenesis (3, 4). A newly described clinicopathological entity, EBV-positive mucocutaneous ulcer (EMU), occurring in immunocompromised patients, has been proposed (4). We describe here a case of EMU presenting with large deep facial ulcers in association with MTX-LPDs, which has not previously been reported in literature.

## CASE REPORT

A 62-year-old woman with polymyositis was treated with low-dose prednisolone (5–10 mg/day) and MTX (5 mg twice a week) for 7 years. Four years before our initial examination, erosive lesions emerged suddenly around her lips and evolved gradually into large ulcers on the mouth, nose and right lower eyelid. Topical anti-bacterial agents, such as gentamicin sulphate, nadifloxacin, and sulfadiazine silver cream, were given by a rheumatologist, with only limited effects. The ulcers progressively enlarged to double the original size and, in November 2007, she was referred to us for clinical assessment of these lesions.

On examination, her body temperature was 36.7°C. Since she felt intolerable pain when opening her mouth, eating was severely disturbed. Several cervical lymph nodes were palpable at a size of 1–1.5 cm. There were five facial ulcers, ranging from 1–6 cm in diameter, each located on the lower lip to jaw, neck, left nasolabial groove, philtrum, and right lower palpebra (Fig. 1A). The ulcers were sharply demarcated and raised on the skin, with mottled telangiectasia and an erythematous hue, as seen on the jaw. Scars were also noted. Laboratory investigations revealed mild elevations of liver enzymes, lactate dehydrogenase (LDH) (291 IU/ml; <208 IU/ml), aspartate transaminase (AST) (38 IU/ml; <30 IU/ml), alanine transaminase (ALT) (40 IU/ml; <30 IU/ml), leucine amino peptidase (78 IU/ml; <43 IU/ml), and a high elevation of C-reactive protein (6.67 mg/dl; <0.1 mg/dl). White blood cell counts fluctuated within the normal range during the course (5,800–8,800/μl) although mild lymphocytopenia was constantly observed (340–582/μl; 1,500–4,000/μl). Serum immunoglobulin G (IgG) levels were low (689 mg/dl; 1,200–2,120 mg/dl), while serum levels of IgA and IgM were normal. The level of soluble interleukin-2 receptor was extremely high (5,834 IU/ml; <534 IU/ml). Cytomegalovirus pp65 (C7-HRP) antigen-positive cells were detected in 94 cells/48,000 cells (normal 0) of peripheral blood mononuclear cells (PBMCs). No anti-EBV-virus capsid antigen IgM (anti-EBV-VCA IgM), anti-EBV-erythrocyte ATP/ADP ratio IgG (anti-EBV-EADR IgG) or anti-EBV-Epstein-Barr nuclear antigen IgG (anti-EBV-EBNA IgG) was detected. EBV-deoxyribonucleic acid (DNA) copy number in the peripheral blood was 1,500 copies/$10^6$ PBMCs (normal <20 copies/$10^6$ PBMCs). The anti-VCA-IgG titre was ×160. β-D glucan levels was 876 pg/ml (<20 pg/ml). These data indicated opportunistic reactivation of cytomegalovirus (CMV), EBV and not-yet-identified fungal infection, presumably due to an underlying immunocompromised status.

Skin histopathology from around the ulcer on the right cheek revealed hyperkeratosis and epidermal inclusion cysts (Fig. 1B). Lymphocytes bearing large nuclei and even Reed-Sternberg (RS) cell-like nuclei had massively infiltrated the dermis and subcutis (Fig. 1C). Large abnormal lymphocytes that clustered around the vessels (Fig. 1D). These large cells were $CD3^-$, $CD15^-$, $CD20^+$, $CD30^+$ and $CD79a^-$, and partially $LMP\text{-}1^+$. Because of similarity in the size and distribution, $CD20^+$ cells, but not $CD3^+$ cells or $CD56^+$ cells, are likely to be EBV-encoded RNA positive

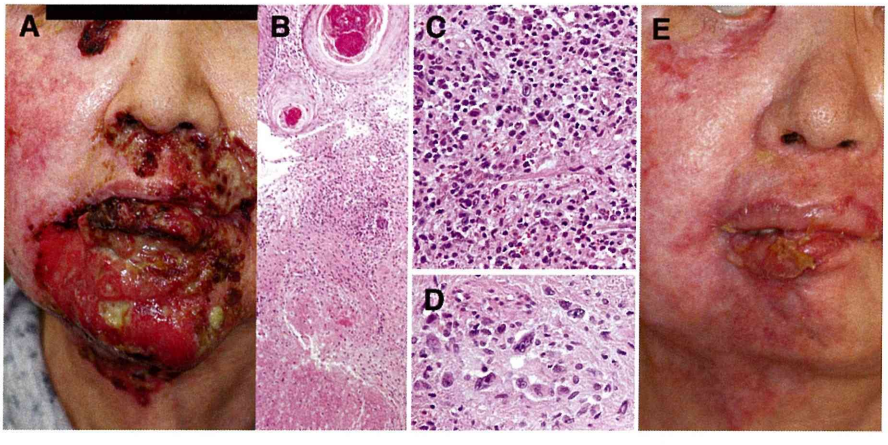


*Fig. 1.* Clinical and histological findings. Skin ulcers of the face, (A) before and (E) after withdrawal of methotrexate (MTX). Skin histopathology of the right cheek (haematoxylin-eosin staining). (B and C) Lymphocytic infiltration in the skin with hyperproliferative epidermal changes was noted (B: ×40; C: ×100, original magnification). (D) Reed-Sternberg cell-like, large abnormal lymphocytes were located near the dermal vessels (×400, original magnification).

 doi: 10.2340/00015555-1274
 ISSN 0001-5555

(EBER$^+$), as identified by *in situ* hybridization analysis. PCR analysis of DNA extracted from the skin sample for spectrotyping assay using a LymphoTrack™ IGH TrackOne™ kit (InVivoScribe Technologies, San Diego, CA, USA) identified a monoclonal spike the size of the immunoglobulin gene D1-6 region, indicating monoclonality of the infiltrating B cells. A diagnosis of EMU, in association with MTX-LPDs, was made. MTX was discontinued and prophylactic treatments with the anti-fungal agents, ganciclovir and combined trimethoprim-sulphamethoxazole, were initiated. Ulcers reduced in size dramatically within 2 weeks and healed within one month (Fig. 1E). However, during this time, the patient's body temperature increased to 39°C and she developed a cough. Chest roentgenograms and bronchoscopic investigation revealed interstitial pneumonitis and bronchial ulcers due to CMV and *Aspergillus* infection. Intensive treatments against these infections, including ganciclovir, valganciclovir, foscarnet and various anti-fungal agents, relieved her symptoms within 3 weeks. A skin biopsy was performed in the vicinity of the first biopsy, and showed sparse lymphocytic infiltration into the dermis. PCR analysis of the skin-derived DNA indicated two substantially lower peaks of different sizes than in the first analysis, confirming that the lymphoma cells had disappeared. EBV-DNA was not detected in the blood. To date, there has been no recurrence of the facial ulcer.

## DISCUSSION

Our patient was diagnosed with EMU in association with MTX-LPDs. EMU is a clinical subtype of B-cell LPDs, which was first proposed by Dojcinov et al. (4) and presents with indolent mucocutaneous ulcers located around the lips and within the oral cavity of immunosuppressed patients. However, it is noteworthy in our case that the skin ulcers were impressively deep and large, unlike ulcers in the previous cases of MTX-associated mucocutaneous ulcers, which may provide a clue for diagnosis of B-cell neoplasms. The infiltration of CD30$^+$ EBV$^+$ large B-cells is a pathognomonic hallmark of EMU (4). Since inflamed ulcers develop gradually and may even partially regress, this condition may be initially misdiagnosed as inflammatory and infectious disorders until a skin biopsy is performed (5).

EBV-associated mucosal lesions in immunosuppressed individuals have previously been reported as LPDs or B-cell lymphomas. Although EMU shares some features with other B-cell lymphomas with RS-like cell infiltrations including classical Hodgkin's lymphoma, T-cell-rich B-cell lymphoma and lymphomatoid granulomatosis, there are distinctive clinical and pathological differences. The majority of RS cells in classical Hodgkin's lymphoma are CD20$^-$ and CD15$^+$ and CD30$^+$, while the neoplastic cells in T-cell-rich B-cell lymphoma are CD20$^+$ and CD14$^-$ or CD30$^-$ (6). Lymphomatoid granulomatosis characteristically shows angiocentric infiltration of lymphocytes (7). Resolution of EMU has been reported in more than 30% of reported cases after restoration of immunosuppression. In the case of MTX-LPDs, especially, tumours were observed to regress dramatically (8–11), a feature also seen in our case. Although several cases of MTX-associated skin ulcers due to the drug toxic effect have been reported (12–14), some of these cases might include EMU associated with MTX treatment.

Since the skin seems easily to be affected by this disease, special attention should be given to skin lesions in immunosuppressed patients (5, 15).

*The authors declare no conflicts of interest.*

## REFERENCES


1. Oyama T, Yamamoto K, Asano N, Oshiro A, Suzuki R, Kagami Y, et al. Age-related EBV-associated B-cell lymphoproliferative disorders constitute a distinct clinicopathologic group: a study of 96 patients. Clin Cancer Res 2007; 13: 5124–5132.
2. Hasserjian RP, Chen S, Perkins SL, de Leval L, Kinney MC, Barry TS, et al. Immunomodulator agent-related lymphoproliferative disorders. Mod Pathol 2009; 22: 1532–1540.
3. Kikuchi K, Miyazaki Y, Tanaka A, Shigematu H, Kojima M, Sakashita H, et al. Methotrexate-related Epstein-Barr Virus (EBV)-associated lymphoproliferative disorder – so-called "Hodgkin-like lesion" – of the oral cavity in a patient with rheumatoid arthritis. Head Neck Pathol 2010; 4: 305–311.
4. Dojcinov SD, Venkataraman G, Raffeld M, Pittaluga S, Jaffe ES. EBV positive mucocutaneous ulcer – a study of 26 cases associated with various sources of immunosuppression. Am J Surg Pathol 2010; 34: 405–417.
5. Steinberg MJ, Herrera AF, Barakat RG. Posttransplant lymphoproliferative disorder resembling a chronic orocutaneous infection in an immunosuppressed patient. J Oral Maxillofac Surg 2004; 62: 1033–1037.
6. Abramson JS. T-cell/histiocyte-rich B-cell lymphoma: biology, diagnosis, and management. Oncologist 2006; 11: 384–392.
7. Katzenstein AL, Doxtader E, Narendra S. Lymphomatoid granulomatosis: insights gained over 4 decades. Am J Surg Pathol 2010; 34: e35–48.
8. Rizzi R, Curci P, Delia M, Rinaldi E, Chiefa A, Specchia G, et al. Spontaneous remission of "methotrexate-associated lymphoproliferative disorders" after discontinuation of immunosuppressive treatment for autoimmune disease. Review of the literature. Med Oncol 2009; 26: 1–9.
9. Miyazaki T, Fujimaki K, Shirasugi Y, Yoshiba F, Ohsaka M, Miyazaki K, et al. Remission of lymphoma after withdrawal of methotrexate in rheumatoid arthritis: relationship with type of latent Epstein-Barr virus infection. Am J Hematol 2007; 82: 1106–1109.
10. Hoshida Y, Xu JX, Fujita S, Nakamichi I, Ikeda J, Tomita Y, et al. Lymphoproliferative disorders in rheumatoid arthritis: clinicopathological analysis of 76 cases in relation to methotrexate medication. J Rheumatol 2007; 34: 322–331.
11. Kojima M, Itoh H, Hirabayashi K, Igarashi S, Tamaki Y, Murayama K, et al. Methtrexate-associated lymphoproliferative disorders. A clinicopathological study of 13 Japanese cases. Pathol Res Pract 2006; 202: 679–685.
12. Warner J, Brown A, Whitmore SE, Cowan DA. Mucocutaneous ulcerations secondary to methotrexate. Cutis 2008; 81: 413–416.
13. Del Pozo J, Martinez W, Garcia-Silva J, Almagro M, Pena-Penabad C, Fonseca E. Cutaneous ulceration as a sign of methotrexate toxicity. Eur J Dermatol 2001; 11: 450–452.
14. Lawrence CM, Dahl MG. Two patterns of skin ulceration induced by methotrexate in patients with psoriasis. J Am Acad Dermatol 1984; 11: 1059–1065.
15. Nemoto Y, Taniguchi A, Kamioka M, Nakaoka Y, Hiroi M, Yokoyama A, et al. Epstein-Barr virus-infected subcutaneous panniculitis-like T-cell lymphoma associated with methotrexate treatment. Int J Hematol 2010; 92: 364–368.

Research article

# Desmoglein 3–specific CD4+ T cells induce pemphigus vulgaris and interface dermatitis in mice

Hayato Takahashi,[1] Michiyoshi Kouno,[1] Keisuke Nagao,[1] Naoko Wada,[1] Tsuyoshi Hata,[1] Shuhei Nishimoto,[1] Yoichiro Iwakura,[2] Akihiko Yoshimura,[3] Taketo Yamada,[4] Masataka Kuwana,[5] Hideki Fujii,[3] Shigeo Koyasu,[3] and Masayuki Amagai[1]

[1]Department of Dermatology, Keio University School of Medicine, Shinjuku-ku, Tokyo, Japan. [2]Center for Experimental Medicine and Systems Biology, Institute of Medical Science, University of Tokyo, Minato-ku, Tokyo, Japan. [3]Department of Microbiology and Immunology, [4]Department of Pathology, and [5]Division of Rheumatology, Department of Internal Medicine, Keio University School of Medicine, Shinjuku-ku, Tokyo, Japan.

**Pemphigus vulgaris (PV) is a severe autoimmune disease involving blistering of the skin and mucous membranes. It is caused by autoantibodies against desmoglein 3 (Dsg3), an adhesion molecule critical for maintaining epithelial integrity in the skin, oral mucosa, and esophagus. Knowing the antigen targeted by the autoantibodies renders PV a valuable model of autoimmunity. Recently, a role for Dsg3-specific CD4+ T helper cells in autoantibody production was demonstrated in a mouse model of PV, but whether these cells exert cytotoxicity in the tissues is unclear. Here, we analyzed 3 Dsg3-specific TCRs using transgenic mice and retrovirus induction. Dsg3-specific transgenic (Dsg3H1) T cells underwent deletion in the presence of Dsg3 in vivo. Dsg3H1 T cells that developed in the absence of Dsg3 elicited a severe pemphigus-like phenotype when cotransferred into immunodeficient mice with B cells from *Dsg3*$^{-/-}$ mice. Strikingly, in addition to humoral responses, T cell infiltration of Dsg3-expressing tissues led to interface dermatitis, a distinct form of T cell–mediated autoimmunity that causes keratinocyte apoptosis and is seen in various inflammatory/autoimmune skin diseases, including paraneoplastic pemphigus. The use of retrovirally generated Dsg3-specific T cells revealed that interface dermatitis occurred in an IFN-γ– and TCR avidity–dependent manner. This model of autoimmunity demonstrates that T cells specific for a physiological skin-associated autoantigen are capable of inducing interface dermatitis and should provide a valuable tool for further exploring the immunopathophysiology of T cell–mediated skin diseases.**

## Introduction

Desmoglein 3 (Dsg3) is a cadherin-type glycoprotein expressed in stratified squamous epithelium, including the skin, oral mucosa, and esophagus, and it plays a critical role in cell-cell adhesion. Dsg3 is the IgG-targeted autoantigen in pemphigus vulgaris (PV) (1). Binding of anti-Dsg3 autoantibodies to epithelial cell surfaces in PV patients and PV model mice inhibits Dsg3 function and leads to the loss of cell-cell adhesion, which manifests clinically as skin blisters and erosions, and histologically as suprabasilar acantholysis (2–4). The antigen-specific autoimmunity in PV makes this disease a valuable model for studying not only autoreactive B cells, but also T cells. Given the importance of the helper function of CD4+ T cells in Ab production (5, 6), autoreactive CD4+ T cells are believed to play critical roles in the pathogenesis of PV. Recently, Dsg3-reactive CD4+ T cell clones were established from *Dsg3*$^{-/-}$ mice (7, 8). Some clones showed helper activity for anti-Dsg3 IgG production and induced the PV phenotype when adoptively transferred with *Dsg3*$^{-/-}$ B cells into *Rag2*$^{-/-}$ mice. Analysis of these clones demonstrated that IL-4 production was critical for Dsg3-reactive T cells in inducing anti-Dsg3 IgG production and the PV phenotype in vivo (7).

T cells are also involved in a rare subset of pemphigus called paraneoplastic pemphigus (PNP). PNP occurs in association with hematopoietic neoplasms and exhibits more complex features than PV (9–11). Anti-Dsg3 and -Dsg1 autoantibodies are detected in PNP, as are autoantibodies against the plakin family, including plectin, desmoplakin I and II, BP230, envoplakin, and periplakin. In addition to acantholysis caused by anti-Dsg3 and -Dsg1 autoantibodies (12), the coexistence of cellular infiltration into lesional epithelial tissue, known as interface dermatitis, is a characteristic histopathological feature in PNP (13). Interface dermatitis is a distinct histological condition in which epidermal basal cell damage occurs subsequent to inflammation at the dermal-epidermal junction. The inflammatory infiltrates consist predominantly of T lymphocytes, and the presence of apoptotic keratinocytes suggests T cell immunity against putative antigens displayed on the surfaces of keratinocytes. Interface dermatitis is observed not only in PNP, but also commonly in lichen planus (LP), lichen sclerosis (LS), toxic epidermal necrolysis/Stevens-Johnson syndrome (TEN/SJS), graft-versus-host disease (GVHD), lupus erythematosus, and other diseases (9, 14–17).

Despite the notion that these skin-infiltrating T cells are autoreactive in nature, there have been few studies of the target antigens, which remain largely unknown, because, unlike Abs, which recognize native proteins, T cell receptors recognize protein peptides in the context of class I or II MHCs. MHC polymorphism and the difficulty in preparing a screening library for peptide-MHC complexes have hampered progress in defining antigen specificity in T cells that infiltrate in inflammatory skin diseases. Consequently, it is unclear whether autoreactive T cells contribute to the pathogenesis of inflammatory skin diseases.

**Authorship note:** Hayato Takahashi and Michiyoshi Kouno contributed equally to this work.

**Conflict of interest:** The authors have declared that no conflict of interest exists.

**Citation for this article:** *J Clin Invest.* 2011;121(9):3677–3688. doi:10.1172/JCI57379.

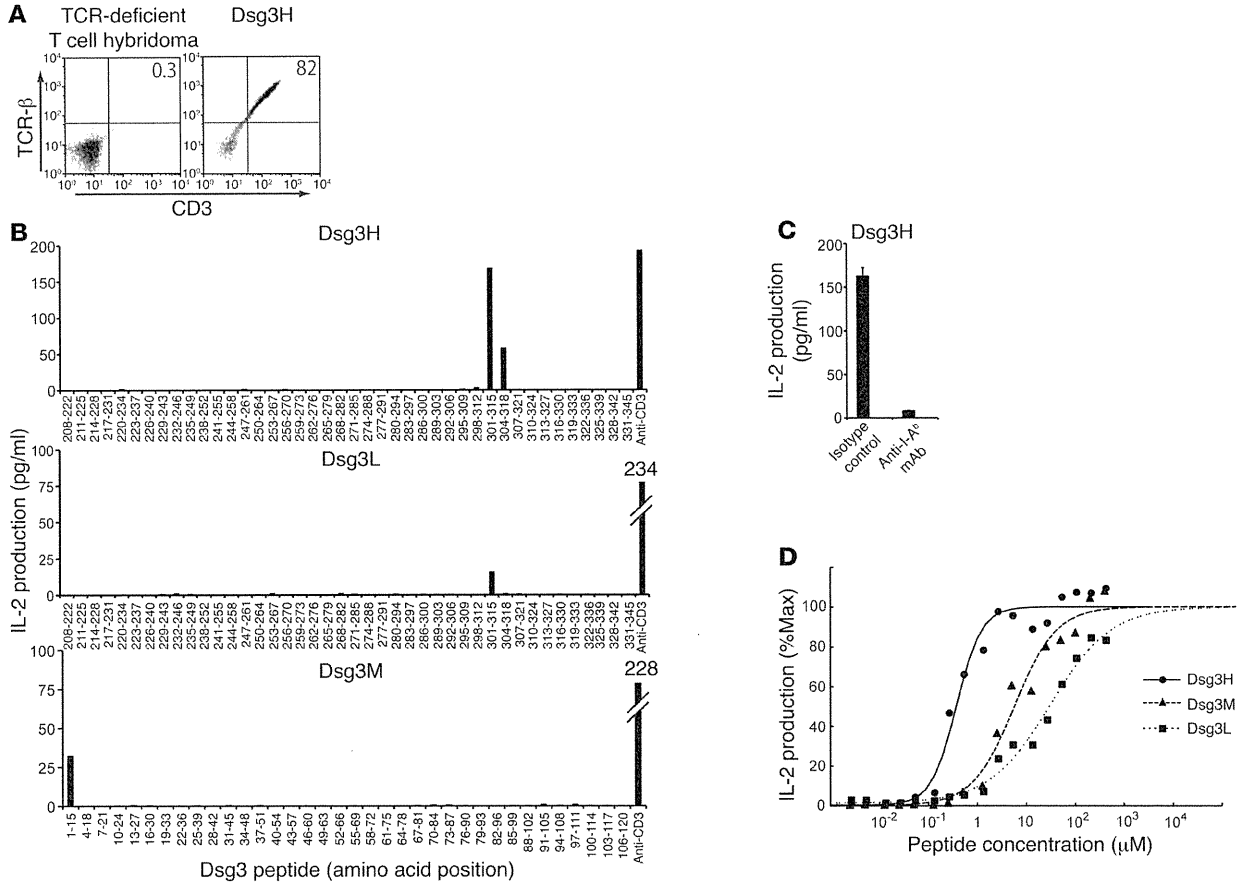


**Figure 1**

Identification of epitope peptides for 3 Dsg3-specific TCRs and a comparison of the differences in their avidities. (**A**) TCR-deficient T cell hybridoma was stably transfected by Dsg3H TCR-α and -β chain genes. Successful coexpression of TCR-β chain and CD3 molecules was subsequently detected by flow cytometry. (**B**) After the Dsg3H, Dsg3L, or Dsg3M hybridoma cell line was cultured with each Dsg3 peptide and irradiated splenocytes or stimulated by anti-CD3 Ab, IL-2 in the supernatant was quantified by ELISA. (**C**) The Dsg3H-transfectant was stimulated with peptide Dsg3(aa 301–315) in the presence or absence of anti-I-$A^b$ Ab. Then, IL-2 was quantified by ELISA. (**D**) Dsg3H (line), Dsg3M (thick dotted line), and Dsg3L (fine dotted line) hybridoma cell lines were cultured with various concentrations of the corresponding peptide and irradiated splenocytes and the supernatant was subjected to IL-2 ELISA. Similar results were obtained in 2 separate experiments.

Here, we report the generation of transgenic mice in which T cells express Dsg3-specific TCRs. Dsg3-specific $CD4^+$ T cells that developed in the absence of Dsg3 caused severe mouse pemphigus when cotransferred with *Dsg3*$^{-/-}$ B cells into *Rag2*$^{-/-}$ mice. Of interest, histological examination of these mice revealed not only epidermal acantholysis (loss of keratinocyte adhesion), but also T cell infiltration of skin that exhibited interface dermatitis. Studies using WT T cells that were retrovirally transduced with Dsg3-specific TCRs revealed that T cells expressing different Dsg3-specific TCRs could induce interface dermatitis and that IFN-γ was a critical factor in inducing this phenotype.

## Results

*Cloning of 3 different TCR genes from Dsg3-reactive T cell clones.* Several Dsg3-reactive T cell clones were previously established from lymph node cells of *Dsg3*$^{-/-}$ mice that were immunized with the extracellular domain of recombinant Dsg3 (7). cDNAs encoding the TCR-α and -β chains were obtained from 3 different T cell clones: 140#27 (AV8S13-J21 and BV6S1-XDX-Jβ1.3), 162#24 (AV20S1-J39 and BV8S1-XDX-Jβ2.7), and 164#2 (AV15S1-J45 and BV6S1-XDX-Jβ2.3). These were subcloned into cassette vectors to enable the expression of both the TCR-α and -β chains (Supplemental Table 1; supplemental material available online with this article; doi:10.1172/JCI57379DS1). The mRNA and amino acid sequences, including the CDR3 regions from these TCR-α and -β chains, are shown in Supplemental Figures 1–6.

*Dsg3-specific TCRs recognize Dsg3 peptides with different avidities.* Vectors constructed to express TCR from 140#27, 162#24, and 164#2 were introduced into TCR-deficient hybridoma cell lines by electroporation to generate Dsg3-specific T cell hybridoma cell lines, referred to as Dsg3H, Dsg3M, and Dsg3L, respectively. TCR-β chain and CD3 molecules were detected on the cell surface of the stable transfectants, indicating that the transduced TCR-α and -β chains were properly assembled on the cell surfaces as a complex with CD3 molecules (Figure 1A and other data not shown). Because the parental T cell clones 140#27 and 164#2 showed proliferative responses on stimulation with the recombinant Dsg3 extracellular domain (aa 210–345), and 162#24 to the Dsg3 extracellular domain (aa 1–119) (7), overlapping Dsg3 peptides covering aa 208–345 and aa 1–120 of

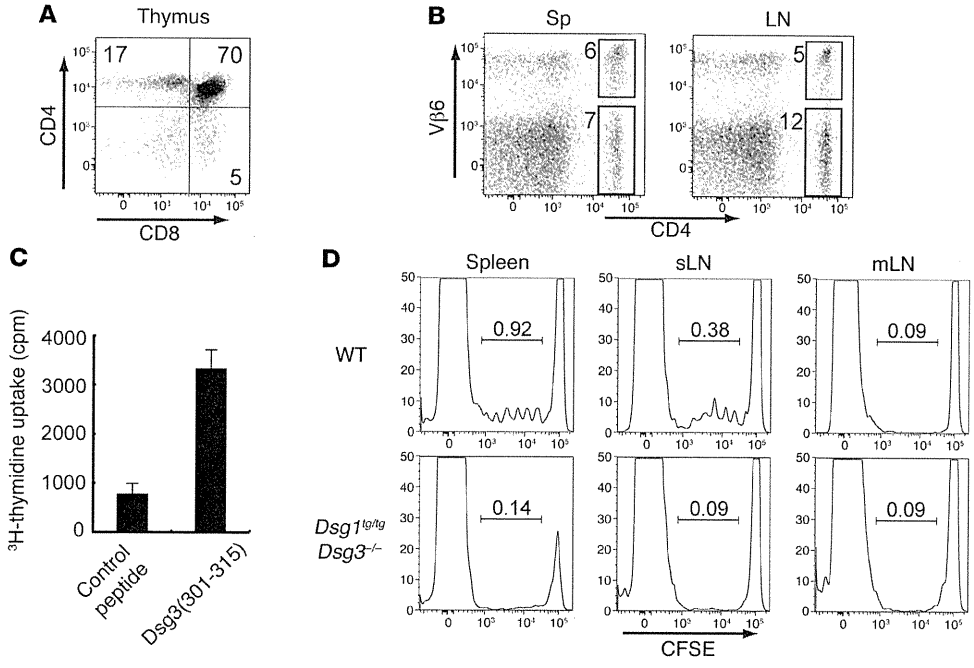


**Figure 2**

Generation of the Dsg3-specific TCR-transgenic mouse, Dsg3H1 mouse, and Dsg3 reactivity of transgenic T cells. (**A**) Thymocytes were stained with anti-CD4 and -CD8 Abs and analyzed by flow cytometry. (**B**) Single-cell suspensions from the spleen and LNs were stained with anti-CD4 and -Vβ6 Abs and analyzed. (**C**) Splenocytes from Dsg3H1 mice were cultured with the peptide Dsg3(aa 301–315) or a control peptide. $^3$H-thymidine incorporation by these splenocytes is shown as the in vitro reactivity against Dsg3 peptide. (**D**) CFSE-labeled CD4$^+$ T cells from Dsg3H1 mice were transferred into B6 WT mice and *Dsg1*$^{tg/tg}$*Dsg3*$^{-/-}$ mice. 3 days later, CFSE dilution was analyzed by flow cytometry after gating CD4$^+$Vβ6$^+$ cells of the spleen, skin-draining LN (sLN), and mesentery LN (mLN) from both recipients. Proportions of dividing cells were shown in each histogram. Similar results were obtained in 2 separate experiments. Data represent mean ± SEM.

Dsg3 were prepared to determine the epitopes for Dsg3H, Dsg3M, and Dsg3L TCR. The Dsg3H hybridoma cell line vigorously produced IL-2 when cocultured with irradiated splenocytes and the peptide Dsg3(aa 301–315), which has the sequence RNKAEFHQSVISQYR (Figure 1B). Interestingly, the Dsg3L hybridoma cell line also produced IL-2 on stimulation with Dsg3(aa 301–315), demonstrating that Dsg3H and Dsg3L recognize identical Dsg3 epitopes. The Dsg3M hybridoma cell line produced IL-2 on stimulation with Dsg3(aa 1–15), which has the sequence EWVKFAKPCREREDN, the endmost peptide of the N-terminus of the mature Dsg3 protein. The reactivity of Dsg3H, Dsg3M, and Dsg3L with the corresponding peptides was inhibited when cultured in the presence of anti-MHC class II blocking Ab (Figure 1C and other data not shown), demonstrating that these TCRs recognized Dsg3 peptides in an I-A$^b$–restricted manner. The synthetic peptides tested here may not necessarily be identical to the ones processed from the native Dsg3 protein. Nevertheless, these TCRs recognized Dsg3 peptides processed in vivo, suggesting that the synthetic peptide Dsg3(aa 301–315) is at least similar, if not identical, to a naturally processed peptide in vivo (Figure 2D). Although appropriate expression of the TCR-α chains of these 3 TCRs could not be confirmed using commercial anti-Vα Abs, this functional assay indicated that both the TCR-α and -β chains were properly expressed.

The avidity of each TCR complex was further evaluated by stimulation with various concentrations of antigenic peptides. All of the Dsg3-specific T cell hybridoma cell lines responded to the corresponding Dsg3 peptides in a dose-dependent manner (Figure 1D). Interestingly, Dsg3H TCR recognized the MHC peptide complex with greater avidity than Dsg3L TCR ($ED_{50}$ 0.37 μM for Dsg3H and 29.3 μM for Dsg3L). Dsg3M TCR showed medium avidity, with an $ED_{50}$ of 5.68 μM, and together with Dsg3H and Dsg3L, provided an interesting set of Dsg3-specific TCRs with differing levels of avidity, at least in the I-A$^b$ background.

*Generation of Dsg3-specific TCR-transgenic mice.* The development of transgenic mice that express Dsg3-specific TCRs should enable a better understanding of the roles of autoreactive T cells in the pathogenesis of pemphigus in vivo. T cell clone 140#27 induced anti-Dsg3 Ab production and the PV phenotype in vivo when cotransferred with *Dsg3*$^{-/-}$ B cells into *Rag2*$^{-/-}$ mice (7). Thus, the TCR from this clone was used to generate TCR transgenic mice, Dsg3H mice. Ultimately, to be able to study the development of autoreactive T cells in detail, it was necessary to select a line of transgenic mice in which T cell development occurred in a manner comparable to that in WT mice. We chose the transgenic line Dsg3-specific transgenic (Dsg3H1) from among several lines because transgenic T cells in Dsg3H1 started to express the TCR-β chain at the DN4 stage in the thymus, as do WT αβ T cells under physiological conditions (Supplemental Figure 7). CD4 single-positive T cells developed in the thymuses of Dsg3H1 mice (Figure 2A). Of the CD4$^+$ population in the spleen and lymph nodes of the Dsg3H1 mouse, 30%–40% were Vβ6$^+$ cells (Figure 2B).

*Transgenic CD4$^+$Vβ6$^+$ T cells from Dsg3H1 mice react to Dsg3.* First, we examined the in vitro reactivity of CD4$^+$Vβ6$^+$ Dsg3H1 T cells to Dsg3. Splenocytes from Dsg3H1 mice were cultured with irradiated

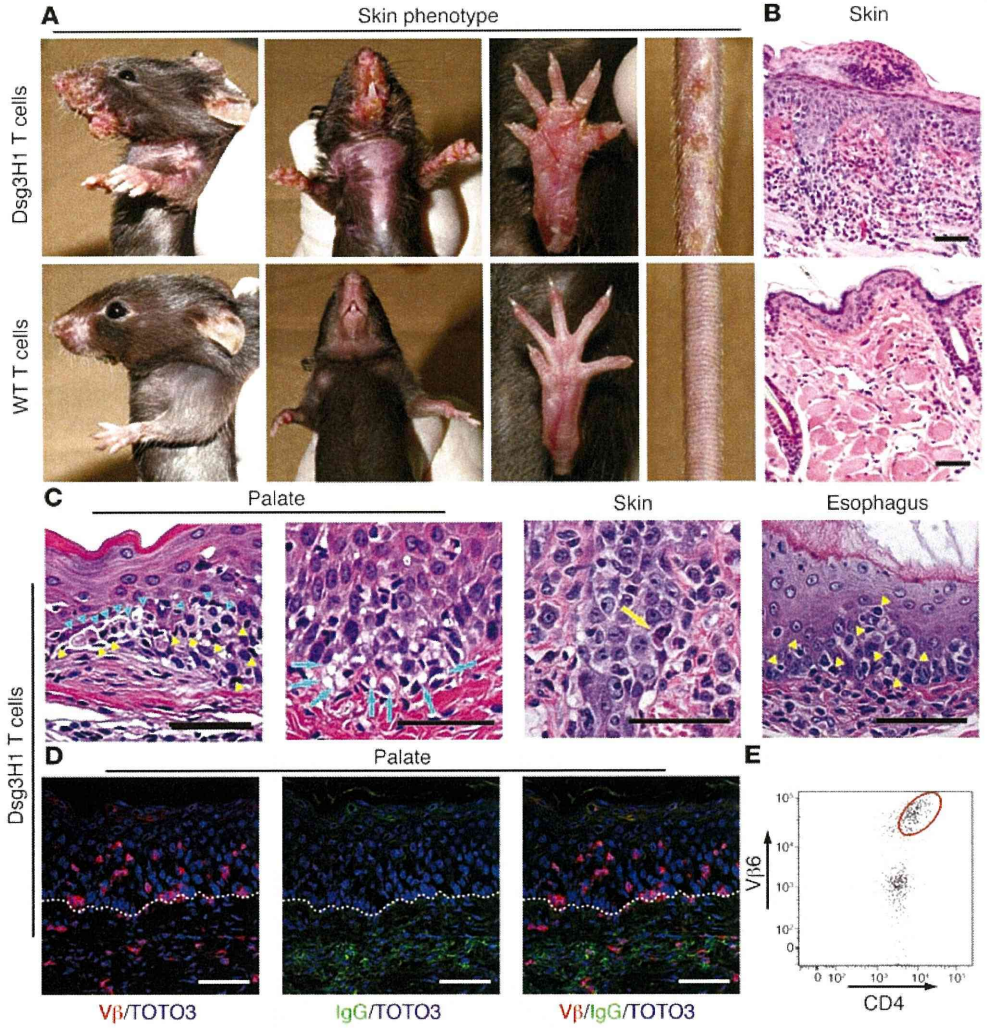


**Figure 3**

Tolerized Dsg3H1 T cells induced interface dermatitis, but not PV. (**A**) The skin phenotype of *Rag2*$^{-/-}$ mice ($n$ = 3 per group) given CD4$^+$Vβ6$^+$ cells from Dsg3H1 mice or CD4$^+$ T cells from C57BL/6 mice in combination with *Dsg3*$^{-/-}$ B cells. Erosive and crusted lesion in the perioral region, upper limbs, paws, and tail and hair loss on the chest were evident (upper panels). (**B**) Pathology of the skin in the recipients given CD4$^+$Vβ6$^+$ cells from Dsg3H1 mice or WT CD4$^+$ T cells. (**C**) Various Dsg3-expressing tissues in the recipients of CD4$^+$Vβ6$^+$ cells from Dsg3H1 mice were stained with H&E. Blue arrowheads indicate degenerated cells in the epithelium. Yellow arrowheads indicate intraepithelial inflammatory cells. Blue arrows indicate liquefaction degeneration in the basal layer of the lesional epithelium. Yellow arrow indicates a degenerated cell well stained with eosin, a so-called Civatte body. (**D**) The palate was stained with anti–TCR-β chain (red) and anti-IgG (green) Abs and TOTO3 (blue). Dotted lines indicate the basement membrane zone. (**E**) A single-cell suspension was prepared from the lesional skin of the recipients given CD4$^+$Vβ6$^+$ cells from Dsg3H1 mice and analyzed by flow cytometry after gating into the CD45$^+$7-AAD$^-$ population. Scale bars: 50 μm.

splenocytes in the presence of the peptide Dsg3(aa 301–315), and their proliferation was analyzed using a $^3$H-thymidine uptake assay. Addition of Dsg3 peptide induced proliferative responses, demonstrating that splenocytes from Dsg3H1 mice contained T cells that were functionally reactive to Dsg3(aa 301–315) ex vivo (Figure 2C).

We confirmed the antigen specificity of Dsg3H1 T cells in vivo. Because APCs present various antigenic peptides, including self antigens in the context of MHC class II molecules (18, 19), we evaluated whether APCs from WT mice were able to stimulate the proliferation of CD4$^+$ Dsg3H1 T cells in vivo. CD4$^+$ Dsg3H1 T cells were labeled with CFSE and then adoptively transferred into C57BL/6 WT mice or *Dsg1*$^{tg/tg}$*Dsg3*$^{-/-}$ C57BL/6 mice. *Dsg1*$^{tg/tg}$*Dsg3*$^{-/-}$ mice express Dsg1, driven by the keratin 5 promoter, which functionally compensates for the loss of Dsg3, leading to better survival in various experimental settings (20). Three days after the transfer, CFSE dilution of CD4$^+$Vβ6$^+$ cells was detected in both the spleen and skin-draining LNs, but not in the mesenteric LNs of C57BL/6 WT mice. Importantly, no CFSE dilution was detected in any of the *Dsg1*$^{tg/tg}$*Dsg3*$^{-/-}$ mice, indicating that CD4$^+$ Dsg3H1 T cells proliferated only in the presence of Dsg3, further ensuring the antigen reactivity of these cells in vivo (Figure 2D).

*Transgenic Dsg3H1 T cells undergo Dsg3-dependent T cell selection.* Despite the forced expression of Dsg3-specific TCR, only 30%–40% of the CD4$^+$ T cells were Vβ6$^+$ in Dsg3H1 mice. Conceivably, the rel-

**Table 1**
Dsg3-specific TCRs and their abilities to induce interface dermatitis in the recipient mice after adoptive transfer of Dsg3-specific T cells with *Dsg3*$^{-/-}$ B cells into *Rag2*$^{-/-}$ mice

| Dsg3-specific TCR, epitope, avidity | T cell source | |
|---|---|---|
| | TCR transgenic mouse | Retroviral transduction |
| Dsg3H, Dsg3(aa 301–315), high | + | + |
| Dsg3M, Dsg3(aa 1–15), medium | ND | + |
| Dsg3L, Dsg3(aa 301–315), low | – | – |

ND, not determined.

atively low number of Vβ6$^+$ cells is due to the presence of tolerance mechanisms in these Dsg3-expressing animals. To determine the effect of the presence or absence of Dsg3 during T cell development, BM cells from Dsg3H1 mice (Ly9.2, I-A$^b$) were transferred into sublethally irradiated 129/Sv WT and 129/Sv *Dsg3*$^{-/-}$ mice (Ly9.1, I-A$^b$) to generate BM chimeric mice, referred to as Dsg3H1→WT mice and Dsg3H1→*Dsg3*$^{-/-}$ mice, respectively (Supplemental Figure 8). Because of the sublethal irradiation dose, efficient adaptation of the donor BM occurs in the presence of recipient hematopoietic cells that are not eradicated by irradiation, allowing the evaluation of Dsg3H1 T cell development as a subpopulation among a diverse repertoire of T cells. The donor Ly9.2$^+$ T cells can be distinguished from recipient Ly9.1$^+$ T cells using an anti-Ly9.1 Ab. Strikingly, in Dsg3H1→*Dsg3*$^{-/-}$ mice, in which Dsg3H1 T cells developed in the absence of Dsg3, Ly9.1$^-$CD4$^+$ Vβ6$^+$ cells constituted over 95% of the donor-derived CD4$^+$ T cells. Under the *Dsg3*$^{+/+}$ condition in Dsg3H1→WT mice, the proportion of Ly9.1$^-$CD4$^+$ Vβ6$^+$ T cells was much decreased, to proportions similar to those of Dsg3H1 mice (Supplemental Figure 9A). These results demonstrated that T cell tolerance mechanisms against Dsg3 exist in WT mice and that Dsg3H1 T cells undergo Dsg3-dependent negative selection in Dsg3H1 mice. However, the incomplete deletion may reflect Dsg3H1 T cells that had "escaped" from the deletion process.

*Tolerance mechanisms inhibit the induction of PV, but not interface dermatitis, by Dsg3H1 T cells.* We questioned whether the Dsg3-reactive CD4$^+$Vβ6$^+$ T cells that were present in the periphery of Dsg3H1 mice, which presumably had escaped the above-described tolerance mechanisms, still had the capacity to induce PV. To determine this, Dsg3H1 T cells were isolated from Dsg3H1 mice directly and cotransferred with *Dsg3*$^{-/-}$ B cells into *Rag2*$^{-/-}$ mice. Fine scales and mild erythema developed on the ears, neck, tail, and soles within 1 week of adoptive transfer; these progressed to erosions and swelling of the arms, perioral region, and trunk (Figure 3A). This phenotype was not observed in the recipients that were cotransferred with simultaneously isolated WT CD4$^+$ T cells and *Dsg3*$^{-/-}$ B cells.

Strikingly, however, no anti-Dsg3 IgG Abs were found in serum from these mice (data not shown). Histopathological studies revealed massive inflammatory cell infiltrates not only in skin, but also in the palate and esophagus, the epithelia of which express Dsg3 (Figure 3, B and C, and Supplemental Figure 10). Lesional epithelia exhibited acanthosis and hyperkeratosis, and keratinocytes undergoing apoptosis and degeneration were observed among the infiltrating lymphocytes. Liquefaction degeneration was observed in the basal cell layers (Figure 3C), where apoptotic keratinocytes resembled Civatte bodies (Figure 3C), as seen in human diseases that involve interface dermatitis (21, 22). These features indeed fulfilled the criteria of human interface dermatitis (Table 1). Immunofluorescence microscopy revealed the infiltration of TCR-β$^+$ T cells in the epidermis (Figure 3D), and a major population of these was identified as CD4$^+$Vβ6$^+$ T cells by flow cytometry (Figure 3E). In contrast with the lymphocyte infiltration, neither suprabasilar acantholysis nor IgG deposition on the surface of keratinocytes was detected (Figure 3, C and D), consistent with the absence of anti-Dsg3 IgG Abs in serum from these mice. Thus, Dsg3H1 T cells that had developed in the presence of Dsg3 did not exert helper activity for B cell autoantibody production to cause PV, but were capable of inducing interface dermatitis, a distinct T cell–mediated inflammation at the dermal-epidermal junction seen in LP, LS, lupus, GVHD, SJS/TEN, PNP, and other diseases.

*Nontolerized Dsg3H1 T cells induce both anti-Dsg3 IgG production and interface dermatitis.* Paradoxically, whereas the parental T cell clone of Dsg3H1 TCR, 140#27, helped *Dsg3*$^{-/-}$ B cells to produce anti-Dsg3 autoantibodies, Dsg3H1 T cells could not. We next asked whether the presence or absence of Dsg3 during T cell development influenced the fate of T cell development in Dsg3H1 mice. 140#27 was originally established from *Dsg3*$^{-/-}$ mice (7). Thus, to mimic this developmental setting, the pathogenic activity of transgenic Dsg3H1 T cells was evaluated using BM chimeric Dsg3H1→*Dsg3*$^{-/-}$ mice. Ly9.1$^-$CD4$^+$ T cells in Dsg3H1→*Dsg3*$^{-/-}$ mice, referred to as Dsg3H1→*Dsg3*$^{-/-}$ CD4$^+$ T cells, showed the CD44$^{lo}$ naive T cell phenotype and expressed the Vβ6 chain (Supplemental Figure 9, A and B). These naive Dsg3H1→*Dsg3*$^{-/-}$ CD4$^+$ T cells were isolated and cotransferred with *Dsg3*$^{-/-}$ B cells into *Rag2*$^{-/-}$ mice (Supplemental Figure 8) and were analyzed 1 week after adoptive transfer. Ly9.1$^-$CD4$^+$ T cells in Dsg3H1→WT mice, referred to as Dsg3H1→WT CD4$^+$ T cells, were used as a control. Because Dsg3H1→WT CD4$^+$ T cells contained approximately 30% of the CD44$^{hi}$ population (memory/activated phenotype; Supplemental Figure 9B), naive T cells were isolated by depleting CD44$^{hi}$ memory cells from the Ly9.1$^-$CD4$^+$ cell population of Dsg3H1→WT mice (Supplemental Figure 9B) and transferred with *Dsg3*$^{-/-}$ B cells into *Rag2*$^{-/-}$ mice (Supplemental Figure 8). The recipient mice that received naive Dsg3H1→*Dsg3*$^{-/-}$ CD4$^+$ T cells and *Dsg3*$^{-/-}$ B cells developed erythma and crusted lesion on the trunk, neck, limbs, face, and paws (Figure 4A). ELISA showed that anti-Dsg3 IgG was produced in these recipient mice (Figure 4B). Living cell staining also demonstrated that IgG from these mice bound to native antigens expressed on the surfaces of the mouse epidermal cell line (Pam cells) (Figure 4C). Consistently, histopathological analysis revealed suprabasilar acantholysis in the palate (Figure 4D). In addition to suprabasilar acantholysis, however, CD4$^+$ T cell infiltration of the epithelium and lamina propria mucosae was observed in the palate. Immunofluorescence analysis demonstrated the coexistence of IgG deposition on the epithelial cell surfaces and Vβ$^+$ T cell infiltration (Figure 4E and Table 2). There were no detectable circulating IgG Abs against desmoplakin, envoplakin, and periplakin in the recipient mice (data not shown). The combination of suprabasilar acantholysis and interface dermatitis observed in this mouse model is similar to the pathological changes observed in human PNP (Figure 4F).

In contrast, anti-Dsg3 IgG was not detected in the recipient mice transferred with naive Dsg3H1→WT CD4$^+$ T cells and *Dsg3*$^{-/-}$ B cells by either ELISA, living cell staining, or immunofluorescence analyses (Figure 4, B, C, and E), and suprabasilar acantholysis by histology was not observed in the palate (Figure 4D). However,

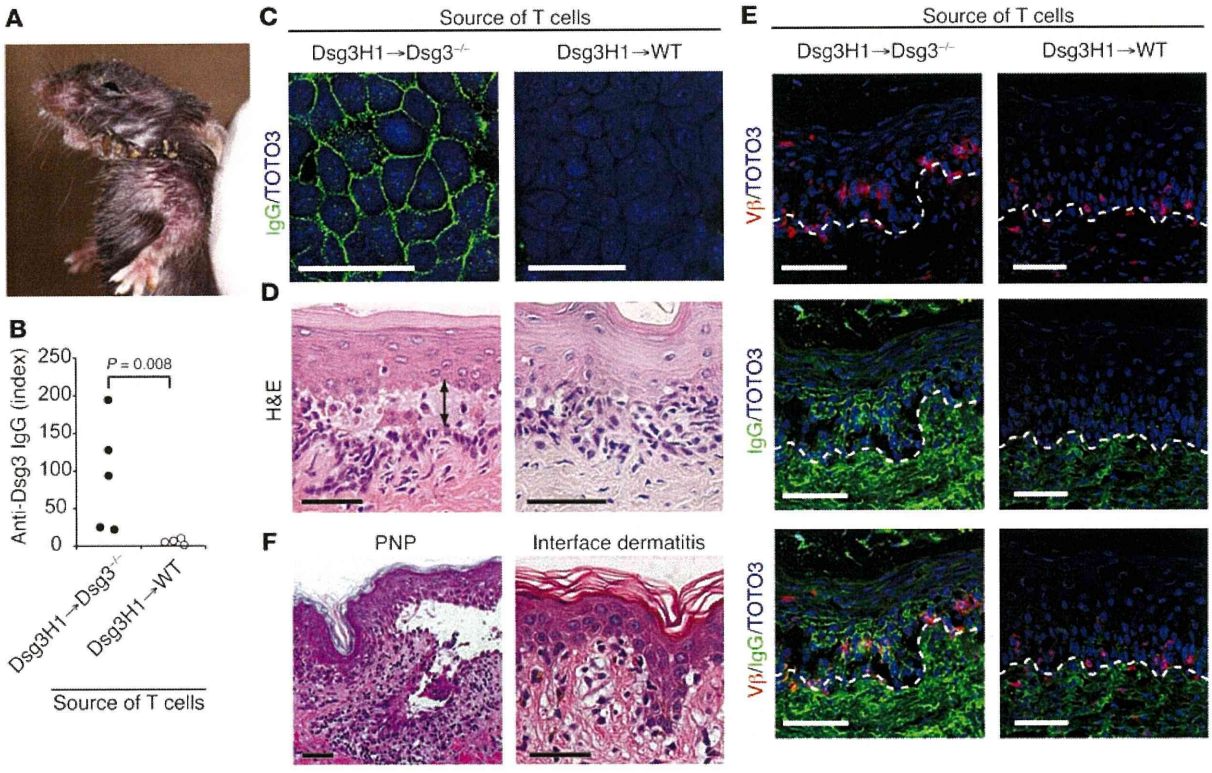


**Figure 4**

Nontolerized Dsg3H1 T cells induce both anti-Dsg3 IgG production and interface dermatitis. BM cells from Dsg3H1 mice (Ly9.2) were transferred into sublethally irradiated 129/Sv WT and *Dsg3*$^{-/-}$ mice (Ly9.1) to generate BM chimeric mice, referred to as Dsg3H1→WT and Dsg3H1→*Dsg3*$^{-/-}$ mice, respectively. Donor-derived naive CD4$^+$Vβ6$^+$CD44$^-$Ly9.1$^-$ cells were enriched from Dsg3H1→WT and Dsg3H1→*Dsg3*$^{-/-}$ mice and were cotransferred with *Dsg3*$^{-/-}$ B cells into *Rag2*$^{-/-}$ mice. (**A**) Skin phenotype in the recipient mice that received donor-derived CD4$^+$ T cells from Dsg3H1→*Dsg3*$^{-/-}$ mice and *Dsg3*$^{-/-}$ B cells. Erythema and crusted lesions were observed in face, neck, and limbs. (**B**) Anti-Dsg3 IgG Ab titers in sera from the recipients were analyzed by ELISA. Statistical analysis was performed using the Mann-Whitney *U* test. (**C**) Sera from the recipients were added to the culture medium of Pam cells. IgG deposition on the cell surfaces was subsequently detected by anti-IgG Ab Alexa Fluor 488. Nuclei were stained with TOTO3 (blue). (**D**) Palates of the recipients were analyzed by H&E staining. The arrow indicates suprabasilar acantholysis. (**E**) Intraepidermal T cells (red) and IgG deposition (green) in the recipient's palate were detected using anti–TCR-β Ab and anti-mouse IgG Ab, respectively. Dotted lines show the basement membrane zone. Similar results were obtained in 2 separate experiments. (**F**) The skin histopathology of PNP and interface dermatitis (GVHD) are shown. Scale bars: 50 μm.

some cell infiltration was observed in the palate of the recipient with naive Dsg3H1→WT CD4$^+$ T cells, and immunofluorescence analysis identified the infiltrating cells as Vβ$^+$ cells (Figure 4E and Table 2). Similar infiltration was observed in the skin and esophagus, where Dsg3 was expressed (data not shown). These results demonstrated that nontolerized Dsg3-specific CD4$^+$ T cells that developed in the absence of Dsg3 are able not only to induce suprabasilar acantholysis via the production of anti-Dsg3 autoantibodies, but are also capable of infiltrating skin directly to cause interface dermatitis, which in combination, showed some findings that are seen in PNP. These results suggest that those Dsg3H1 T cells that are capable of inducing PV are highly reactive with Dsg3 and are negatively selected in the *Dsg3*$^{+/+}$ environment.

*Avidity-dependent induction of interface dermatitis by Dsg3-specific T cells.* Because we had cloned 3 different Dsg3-specific TCRs with differing avidities, this gave us an opportunity to determine whether different TCRs specific for Dsg3 could induce interface dermatitis and to evaluate any relationship between TCR avidity and clinical severity. To determine this, we retrovirally transduced WT CD4$^+$ T cells with Dsg3-specific TCRs Dsg3H, Dsg3M, or Dsg3L, each with differing avidities for Dsg3 (see Figure 1D). By performing transduction on WT CD4$^+$ T cells, it is possible to circumvent TCR avidity–specific events that may occur during thymic selection. WT CD4$^+$ T cells were retrovirally transduced with Dsg3H TCR to generate rvDsg3H T cells, which properly acquired Dsg3 reactivity, shown by the robust IL-2 production on stimulation with Dsg3(aa 301–315) (Supplemental Figure 11). When rvDsg3H T cells were transferred with or without *Dsg3*$^{-/-}$ B cells into *Rag2*$^{-/-}$ mice, the recipient mice developed erosive and crusted lesions on the ears, neck, periorbital region, paws, and tail (Figure 5A). Histopathological analysis revealed interface dermatitis in the skin, palate, and esophagus (Figure 5A and other data not shown). Interface dermatitis was not observed in non–Dsg3-expressing tissues, including the liver and small and large intestines (Supplemental Figure 12). Furthermore, recipients to which *Dsg3*$^{-/-}$ B cells were also transferred showed no anti-Dsg3 IgG production or PV phenotype (Supplemental Figure 13). Control animals that received CD4$^+$ T cells transduced with control retro-

**Table 2**
Phenotype of the recipient mice after adoptive transfer of BM chimera-derived Dsg3H1 cells with *Dsg3*$^{-/-}$ B cells into *Rag2*$^{-/-}$ mice

| | BM chimera as T cell source | |
|---|---|---|
| **Phenotype** | **Dsg3H1→WT** | **Dsg3H1→*Dsg3*$^{-/-}$** |
| IgG production[A], acantholysis | – | + |
| Interface dermatitis | + | + |

[A]Dsg3-specific Ab.

virus, rvGFP T cells, did not develop any phenotype (Figure 5A). Overall, the phenotype induced by rvDsg3H T cells was nearly identical to that of Dsg3H1 T cells.

Next, we generated rvDsg3M (medium avidity) and rvDsg3L (low avidity) T cells, and transferred them into *Rag2*$^{-/-}$ mice with no B cells. Whereas mice that received rvDsg3M subsequently developed scaly erythema, comparable to mice that received rvDsg3H, mice that received rvDsg3L T cells did not develop any skin abnormalities (Figure 5, B and C). The histopathology of the lesional skin induced by rvDsg3H and rvDsg3M revealed interface dermatitis (Table 1). Consistent with earlier experiments, no lesion was seen in non–Dsg3-expressing tissues (Supplemental Figure 12).

To confirm the nonpathogenic nature of Dsg3L TCR in inducing interface dermatitis, a Dsg3L TCR transgenic mouse (i.e., the Dsg3L3 mouse) was evaluated. More than 90% of the CD4$^+$ T cells expressed Vβ6 in the spleen and LNs of Dsg3L3 mice (Supplemental Figure 14A). CD4$^+$Vβ6$^+$ T cells from Dsg3L3 transgenic mice were cotransferred with *Dsg3*$^{-/-}$ B cells into *Rag2*$^{-/-}$ mice, but unlike those that received Dsg3H1 T cells, the Dsg3L3 recipient mice did not develop any abnormalities, consistent with the results obtained with the retroviral system (Table 1 and Supplemental Figure 14B).

Thus, T cells expressing Dsg3-specific TCRs with high and medium avidity, but not those with low avidity, were capable of eliciting interface dermatitis. These results collectively demonstrated that interface dermatitis could be induced in an antigen-specific and a TCR avidity–dependent manner by Dsg3-specific CD4$^+$ T cells.

*IFN-γ–dependent induction of interface dermatitis by Dsg3-specific T cells.* To further understand the molecular events that influenced Dsg3H1 T cells to elicit different phenotypes depending on their exposure to Dsg3 during developmental processes, cytokine analyses were performed to clarify which T helper subset the Dsg3H1 T cells had differentiated into in vivo. Naive Dsg3H1 T cells that were cotransferred with *Dsg3*$^{-/-}$ B cells into *Rag2*$^{-/-}$ mice were isolated ex vivo after disease elicitation and were analyzed for IFN-γ, IL-4, IL-17A, and Foxp3. Dsg3H1→*Dsg3*$^{-/-}$ CD4$^+$ T cells and Dsg3H1→WT CD4$^+$ T cells were compared (Supplemental Figure 8) because these T cells induced both autoantibody production and interface dermatitis, or only interface dermatitis, respectively (Table 2).

Whereas IFN-γ was the predominant cytokine produced by Dsg3H1 T cells (Ly9.1$^-$CD4$^+$Vβ6$^+$) isolated from the spleens and LNs of both groups, Dsg3H1 T cells isolated from the skin-draining LNs of Dsg3H1→*Dsg3*$^{-/-}$ mice deviated more toward IL-4 production and expressed relatively lower levels of IFN-γ (Figure 6A). Interestingly, whereas a fraction of Dsg3H1→WT CD4$^+$ T cells had differentiated into IL-17A–expressing T cells, this was not observed in Dsg3H1→*Dsg3*$^{-/-}$ CD4$^+$ T cells (Figure 6B). Foxp3-expressing Dsg3H1 T cells were found in similar ratios in the spleen and skin-draining LNs from both groups. It seems likely that the presence or absence of an autoantigen influences T cell development and diversifies T cell properties, such as antigen reactivity, leading to striking differences in cytokine deviation and phenotypic outputs.

It caught our strong interest that in settings where interface dermatitis was the predominant phenotype, both IFN-γ– and IL-17A–producing Dsg3H1 T cells were detected, suggesting that these cytokines played important roles in interface dermatitis. To determine this, we took advantage of the retroviral expressing system, and CD4$^+$ T cells isolated from *Ifng*$^{-/-}$ and *Il17a*$^{-/-}$ mice were transduced to generate *Ifng*$^{-/-}$ or *Il17a*$^{-/-}$ rvDsg3H T cells. Within 3 weeks after the adoptive transfer of WT rvDsg3H T cells and *Il17a*$^{-/-}$ rvDsg3H T cells, *Rag2*$^{-/-}$ mice exhibited skin inflammation, showing scale, crusts, and erythema. Strikingly, however, *Ifng*$^{-/-}$ rvDsg3H T cells failed to elicit any abnormalities (Figure 6C). The histopathology of the skin lesions elicited by WT and *Il17a*$^{-/-}$ rvDsg3H T cells revealed typical interface dermatitis, while the skin of mice transferred with *Ifng*$^{-/-}$ rvDsg3H T cells showed no inflammatory infiltrate (Figure 6D). These findings demonstrated that IFN-γ, but not IL-17A, is the key cytokine produced by Dsg3-specific T cells that causes interface dermatitis.

## Discussion

We generated Dsg3-specific TCR transgenic mice to analyze the development and roles of autoreactive CD4$^+$ T cells in PV. Bone marrow transplantation experiments demonstrated Dsg3 tolerance mechanisms in vivo. When Dsg3H1 T cells that developed in the absence of Dsg3 were cotransferred with *Dsg3*$^{-/-}$ B cells into *Rag2*$^{-/-}$ mice, these mice developed a severe skin phenotype mimicking PNP. Unexpectedly, in addition to Ab production by B cells, direct infiltration of Dsg3H1 T cells was seen in the skin, resulting in histological features that recapitulated interface dermatitis, a phenomenon that is not seen in PV, but in PNP. Retrovirally generated Dsg3H T cells showed that interface dermatitis could be induced independently of B cells, in an IFN-γ– and TCR avidity–dependent manner, indicating that autoimmunity by CD4$^+$ T cells directed against a defined physiological epidermal antigen is sufficient to cause interface dermatitis.

Interface dermatitis exhibits degenerative changes at the dermal-epidermal junction that are accompanied by lymphocytic infiltration (22). Interface dermatitis is divided into 2 subtypes: vacuolar type and lichenoid type (lichenoid dermatitis). Vacuolar types shows small vacuolar spaces at the dermal-epidermal junction, often leaving the junction indistinct. Leukocyte infiltration in this type may not be prominent. On the other hand, lichenoid types show a dense, band-like infiltrate of inflammatory cells, which consists mostly of lymphocytes, in the superficial dermis. Histological findings observed in the skin lesions of our model mice showed interface dermatitis with lymphocytic infiltrations that were not as dense as the band-like infiltration of the lichenoid type and thus more resembled the vacuolar type interface dermatitis, which is found in the original histological description for patients with PNP (9).

Interface dermatitis is observed in various inflammatory conditions of the skin and mucous membranes, including LP, LS, TEN/SJS, GVHD, lupus, and PNP. The infiltrating lymphocytes in LP lesions have been reported to be a mixture of CD4$^+$ and CD8$^+$ T cells (23), which appear, at least histologically, to "attack" the epidermal keratinocytes, causing apoptosis and obscuring the dermal-epidermal junction. It has been described that cytotoxic CD8$^+$ T cells are capable of directly injuring keratinocytes and thus play a central role in interface dermatitis (24, 25). Although there are very few reports that have studied the role of CD4$^+$ T cells in interface dermatitis, one study has

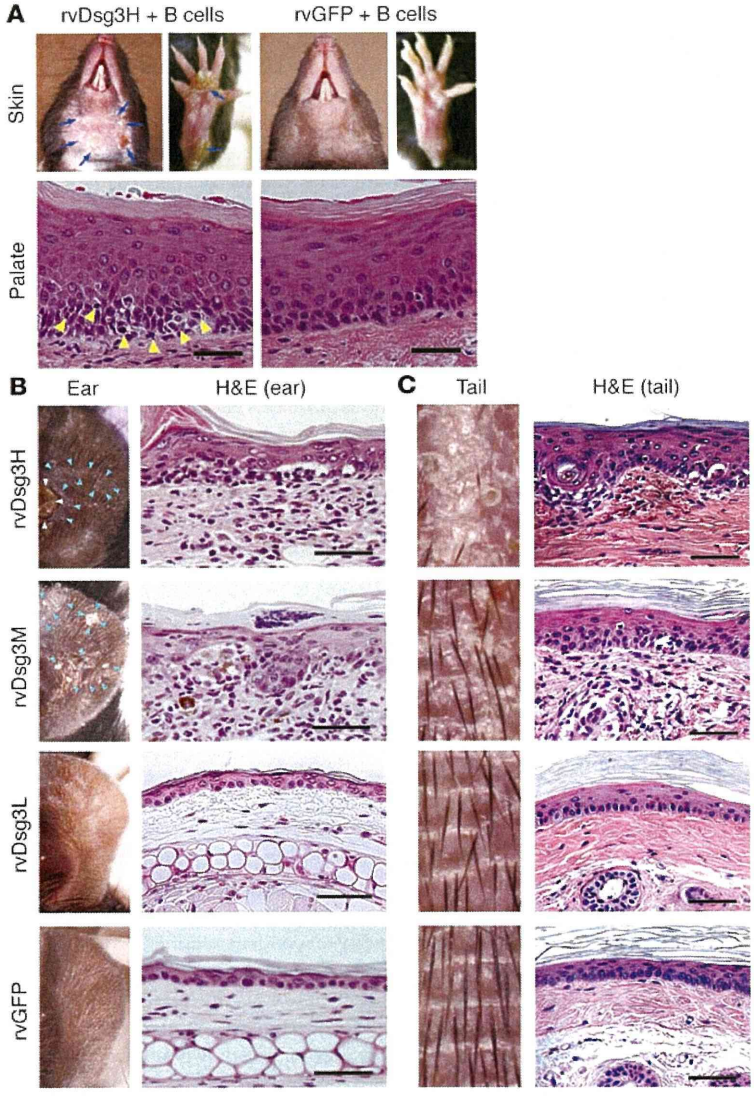


**Figure 5**

Avidity-dependent induction of interface dermatitis by retrovirally transduced Dsg3-specific T cells. Dsg3-specific T cells, including rvDsg3H, rvDsg3M, and rvDsg3L T cells, were generated by retroviral transduction of Dsg3H, Dsg3M, and Dsg3L TCRs into WT $CD4^+$ T cells, respectively. Control T cells, rvGFP T cells, were generated using control retrovirus. (**A**) The skin phenotype and histopathology of the palate from the recipient mice given rvDsg3H T cells and rvGFP T cells in combination with *Dsg3*$^{-/-}$ B cells. Blue arrows show erosive and crusted lesions. Yellow arrowheads indicate inflammatory cell infiltration. (**B** and **C**) rvDsg3H, rvDsg3M, rvDsg3L, and rvGFP T cells were transferred into *Rag2*$^{-/-}$ mice. 4 weeks later, the skin phenotype and histopathology of the ears (**B**) and tails (**C**) were observed. White arrowheads indicate a crusted lesion. Blue arrowheads indicate scaly lesions. Scale bars: 50 μm. Similar results were obtained from 2 independent experiments.

clearly demonstrated that $CD4^+$ T cells alone can injure keratinocytes (26). The cytotoxic effector function of $CD4^+$ T cells has been observed in other animal models, including EAE, with results that are also consistent with ours in terms of tissue injury by $CD4^+$ T cells (27). However, more fundamental questions, such as which population of T cells plays the initial role in triggering interface dermatitis and what proportion of infiltrating $CD4^+$ and $CD8^+$ T cells are specific to certain antigens in skin, remain unresolved. Thus, our experimental autoimmune dermatitis (EAD) model described in this study will provide a valuable tool to clarify such unsolved pathophysiological mechanisms of T cell–mediated skin diseases.

Despite the long-standing notion that these lymphocytes might recognize skin-associated autoantigens, strong evidence for autoimmunity and putative autoantigens is lacking. Interestingly, however, in LS and LP, both of which exhibit interface dermatitis, autoantibodies against extracellular matrix protein 1 (28) and type XVII collagen (29) have been reported, suggesting the existence of autoimmunity in these patients, further implying the possibility that skin-infiltrating T cells might also recognize the same autoantigen. $CD8^+$ T cell lines established from the lesional skin of LP patients exerted cytotoxic activity against immortalized autologous keratinocytes, supporting the involvement of skin-targeted autoimmunity in the development of interface dermatitis (30).

Likewise, the autoantibody targets in PNP are well characterized, but the relative importance of T cell immunity in the pathology and nature of the autoantigen were unclear. The dermatitis observed in our EAD model is a $CD4^+$ T cell response. Thus, it does not fully recapitulate the immunity seen in PNP, in which Ab targets are not restricted to Dsg3, and $CD8^+$ T cells also contribute to the pathogenesis. Nevertheless, mice that were cotransferred with Dsg3H1 T cells and *Dsg3*$^{-/-}$ B cells exhibited PNP-like clinical and pathological features, including both acantholysis and interface dermatitis, resulting in a rapidly progressive course with high mortality. The coexistence of humoral immunity against Dsg3 and interface dermatitis is a phenotypic combination unique to PNP. The results of our murine study imply, for what we believe is the first time, that T cell immunity against Dsg3, among other targets, might exist in human PNP. The finding that direct tissue infiltration of T cells that recognize a specific skin-associated antigen leads to interface dermatitis extends its significance not only to Dsg3 and PV or PNP, but also to other diseases that display interface dermatitis and provides impetus for the further characterization of T cell–mediated inflammatory skin diseases.

Recent research has revealed new subsets of helper T cells and critical cytokines that induce specific responses, including autoimmunity. Th1 and Th17 differentiation and cytokines that support the development of helper T cell subsets, such as IL-12 and IL-23, have been investigated intensively in the context of autoimmune disease models. Th17 cells are important for disease development in collagen-induced arthritis (31–35). In contrast, Th1 cells have been reported to be critical for autoimmune diabetes (36–38). Furthermore, in EAE, conflicting results have been reported and the central role of a particular T helper subset in the induction of EAE is controversial (39–41). This evidence emphasizes that each autoimmune disease may involve differing mechanisms and the pathological mechanisms of each disease must be investigated carefully.

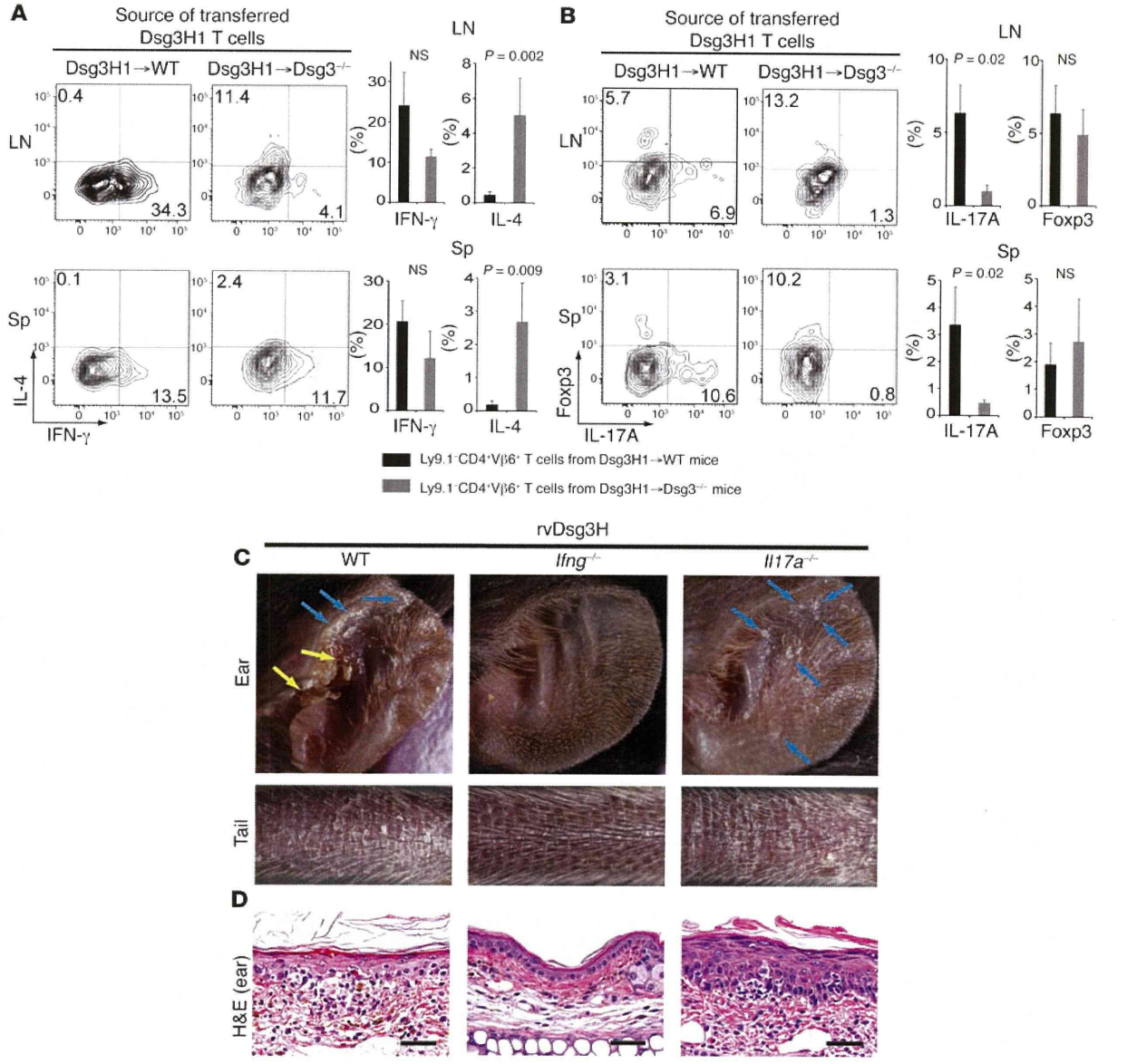


**Figure 6**

Dsg3-specific T cells induce interface dermatitis in an IFN-γ–dependent manner. (**A** and **B**) Naive Dsg3H1→WT or Dsg3H1→*Dsg3*$^{-/-}$ CD4$^+$ T cells were transferred with *Dsg3*$^{-/-}$ B cells into *Rag2*$^{-/-}$ mice. More than 6 days later, LN and spleen were collected and used to make a single-cell suspension, which was then treated with PMA, ionomycin, and brefeldin A, and flow cytometric analysis examined the expression of IFN-γ versus IL-4 (**A**) and IL-17A versus Foxp3 (**B**). Representative contour plots are shown after gating into the CD4$^+$Vβ6$^+$7-AAD$^-$ population. The quadrants were set based on the results of staining with isotype control Abs. Black bars represent the average for Ly9.1$^-$CD4$^+$Vβ6$^+$ T cells from Dsg3H1→WT mice ($n = 6$). Gray bars represent the average for Ly9.1$^-$CD4$^+$Vβ6$^+$ T cells from Dsg3H1→*Dsg3*$^{-/-}$ mice ($n = 6$). Error bars indicate the SEM. Statistical comparison was made using the Mann-Whitney *U* test. (**C** and **D**) CD4$^+$ T cells were isolated from WT, *Ifng*$^{-/-}$, or *Il17a*$^{-/-}$ mice and retrovirally transduced with Dsg3H TCR and transferred into *Rag2*$^{-/-}$ mice. 3 weeks later, the macroscopic phenotype (**C**) and histopathology of the skin (**D**) were observed. Yellow arrows indicate crusted lesions in the ear. Blue arrows indicate scaly lesions. Scale bars: 50 μm. Similar results were obtained from 2 independent experiments.

In our EAD model, the importance of IFN-γ, but not IL-17A, was clearly demonstrated in the induction of interface dermatitis caused by Dsg3-specific T cells. This result is consistent with a previous study, in which H2K$^b$ donor cells from *Il17a*$^{-/-}$ mice, when transferred into H2K$^{b/d}$ recipients, induced GVHD to an extent similar to *Il17a*$^{+/+}$ donor cells (42). However, it is still unclear whether IFN-γ directly acts against keratinocytes to cause tissue destruction or whether IFN-γ acts on T cells themselves to acquire cytotoxic activity. In a model of autoimmune diabetes utilizing NOD mice, IFN-γ was important to induce surface expression of FasL in β cells, which subsequently underwent apoptosis through Fas expressed by activated CD4$^+$ T cells (43). Furthermore, require-

ment of IFN-γ for induction of interface dermatitis implies that other Th1-associated molecules will be critically involved in this model. In addition to IFN-γ, IL-12 and IL-27 play pivotal roles in Th1 differentiation (44, 45). These cytokines participate in activation of molecules such as Jak1 and -2, and STAT1 and -4, all of which are important components of the signaling cascade that induces T-bet expression as well as IFN-γ expression or amplification. These critical molecules in Th1 differentiation may be potential targets to modulate disease activity, and our EAD model should provide a useful tool for in-depth evaluation.

Reported mouse models of TEN (46) and GVHD-like disease (47) target neoantigens in which transgenic mice that express membrane-bound ovalbumin, driven by the keratin 5 or 14 promoters, are transferred with OVA-specific $CD8^+$ T cells from OT-I mice. These mice demonstrated a role for $CD8^+$ T cells in inducing the TEN or GVHD-like phenotype and exhibited interface dermatitis on histology. Although $CD4^+$ T cells are likely involved in helping $CD8^+$ T cells, the roles of $CD4^+$ T cells in these models are unclear. Another report showed a local interface dermatitis model in which $CD5^+CD8^-$ allo-Ia-reactive T cell clones were injected subcutaneously and demonstrated that the immune response against the allo–MHC class II antigen was capable of inducing interface dermatitis (26). The Dsg3-specific TCRs we used are MHC class II–restricted, and these $CD4^+$ T cells were also capable of inducing interface dermatitis. Together, these results demonstrated that $CD4^+$ T cells are sufficient to induce interface dermatitis, at least in the acute phase, and suggest that MHC class II–expressing cells are important cell components in the pathological process.

A major issue in using neoantigen transgenic mice to analyze autoimmune responses is that the level of antigen expression cannot be controlled. Because these are nonfunctional molecules, it is possible that such molecules do not undergo physiological turnover or processing, including degradation and recycling. Studies of the immune reaction against neoantigens may not necessarily reflect the immune reaction against physiological antigens. We believe that the significance of the EAD that we report here lies in the fact that a physiological and functional molecule, which is expressed only in the skin and mucous membranes, is targeted. Dsg3 is also expressed in the thymus by Aire-expressing medullary thymic epithelial cells, and this may influence the output of immune reactions (48). Thus, the use of a physiological antigen as a target antigen of the autoimmune reaction may be important in analyzing autoimmunity. In this regard, Dsg3-specific TCR transgenic mice should provide a useful tool for exploring the development of autoreactive T cells in the thymus, as well as their maintenance or regulation in the periphery. How and where these cells interact with antigen-presenting cells and the processes by which they find their targets are fundamental, important questions in the context of not only PV and PNP, but also in the array of T cell–mediated inflammatory skin diseases that exhibit interface dermatitis.

In conclusion, we generated TCR transgenic mice with autoreactive $CD4^+$ T cells that are specific for Dsg3, a physiological autoantigen expressed by epidermal keratinocytes. The finding that $CD4^+$ T cells specific for a single skin-associated antigen could induce a PNP-like phenotype or interface dermatitis sheds light not only on the pathophysiology of pemphigus, but also on a range of other T cell–mediated inflammatory skin diseases with as-yet-undefined target antigens. This experimental model of autoimmune dermatitis should deepen our understanding of the immunopathophysiology of T cell–mediated skin diseases and provide impetus for investigating targeted autoantigens in human T cell–mediated skin diseases that exhibit interface dermatitis.

## Methods

*Mice.* C57BL/6 (H-$2^b$, Ly-9.2) and 129/Sv mice (H-$2^b$, Ly-9.1) were purchased from CLEA Japan and Sankyo Labo Service Corporation. C57BL/6 *Rag2*$^{-/-}$ mice were purchased from the Central Institute for Experimental Animals (Tokyo, Japan). *Dsg3*$^{-/-}$ mice with a mixed 129/Sv and C57BL/6J genetic background and 129/Sv *Dsg3*$^{-/-}$ mice were obtained by mating male and female *Dsg3*$^{-/-}$ mice (Jackson Laboratory) (49). *Dsg1*$^{tg/tg}$*Dsg3*$^{-/-}$ mice with a C57BL/6 background were generated as described elsewhere (20). *Ifng*$^{-/-}$ mice were purchased from Jackson Laboratory. *Il17a*$^{-/-}$ mice were generated as described previously (42).

The animals were housed under specific pathogen–free conditions. The Keio University Ethics Committee for Animal Experiments approved all of the experiments in this study.

*DNA construct for Dsg3-reactive TCR expression.* Rearranged genes including the variable and junctional regions of the TCR-α and -β chains of a Dsg3-reactive T cell clone, 140#27 (Vα8-Jα21, Vβ6-Dβ1-Jβ1.3) (7), were obtained by RT-PCR using the following primers: Vα-Jα region, forward 5′-TCTCCCGGGTGCACTCAAGGACCAAGTGT-3′ (the *Xma*I site is underlined), reverse 5′-TTGGCTTCACTGTGAGCACGGTCCCA-3′; Vβ-Dβ-Jβ region, forward 5′-GTCTCGAGTTTCTCTTTTAACTAACTAATGCCC-3′ (*Xho*I), reverse 5′-CTACAACAATGAGCCGGCTTCCTT-3′. Jα21 or Jβ1.3 genes with an intron at their 3′ terminus were obtained from genomic DNA by PCR using the following primers: Jα21 intron, forward 5′-GGGGATGGGACCGTGCTCACAGTG-3′, reverse 5′-GCGCGGCCGCCCTGCCAGGAAGTCTAGTCAAAA-3′ (*Not*I); Jβ1.3 intron, forward 5′-GGAGAAGGAAGCCGGCTCATTGT-3′, reverse 5′-GCCCGCGGCGTAGGACTGTGAACAGTACAT-3′ (*Sac*II). The Vα-Jα and Vβ-Dβ-Jβ genes were linked with the Jα intron and Jβ intron to obtain Vα-Jα intron and Vβ-Dβ-Jβ intron genes, respectively, (Supplemental Figures 1 and 2) by linkage PCR. The genes of the TCR-α and -β chains of a Dsg3-reactive T cell clone, 162#24 (AV20S1-J39 and BV8S1-XDX-Jβ2.7), were obtained similarly by RT-PCR and linkage PCR using the following primers: Vα-Jα region, forward 5′-GCCCGGGGGAGAGATAACTCAAAGCTTCAGAGAAGA-3′ (*Xma*I), reverse 5′-GAGGTCTGACTCTCAAAATGGTTCCCAAGCCAAA-3′; Vβ-Dβ-Jβ region, forward 5′-GCTCGAGTAGTTCTGAGATGGGCTCCAGACTCTT-3′ (XhoI), reverse 5′-CTAAAACCGTGAGCCTGGTGCCGGGACCGAAGTA-3′. J39 or Jβ2.7 genes with an intron at their 3′ terminus were obtained from genomic DNA by PCR using the following primers: J39 intron, forward 5′-CTATGCAAACAAGATGATCTTTGGCTTGGGAA-3′, reverse 5′-GCCGCGGTCCAAGCTGTGGGCCACACCAGTGAATTT-3′ (*Sac*II); Jβ2.7 intron, forward 5′-ATGAACAGTACTTCGGTCCCGGCACCAGGCTCA-3′, reverse 5′-GCCGCGGCCCACCCAGTGCATGCATACCTCAGAGA-3′ (*Sac*II). Then, Vα-Jα and Vβ-Dβ-Jβ genes were linked with the Jα intron and Jβ intron to obtain Vα-Jα intron and Vβ-Dβ-Jβ intron genes, respectively. The genes of the TCR-α and -β chains of a Dsg3-reactive T cell clone, 164#2 (AV15S1-J45 and BV6S1-XDX-Jβ2.3), were obtained similarly by RT-PCR and linkage PCR using the following primers: Vα-Jα region, forward 5′-GCCCGGGCTTGCATGGCAAGAGATTGCAAGT-3′ (*Xma*I), reverse 5′-TTGGAGTCACAGTTAAGAGAGTTCCTTT-3′; Vβ-Dβ-Jβ region, forward 5′-GTCTCGAGTTTCTCTTTTAACTAACTAATGCCC-3′ (*Xho*I), reverse 5′-CGAGAACAGTCAGTCTGGTTCCT-3′. J45 or Jβ2.3 genes with an intron at their 3′ terminus were obtained from genomic DNA by PCR using the following primers: J45 intron, forward 5′-GGAGGCAGCAATTACAAACTGACAT-3′, reverse 5′-GCCGCGGCTGGATCCTGTATTCAATGTGCCTCCCT-3′ (*Sac*II); Jβ2.3 intron, forward 5′-GCAGAAACGCTGTATTTTGGCT-3′, reverse 5′-GCCGCGGCGAGGAGCCGAGTGCCTGGCCCAAA-3′ (*Sac*II).

Genes for the TCR-α and -β chains of 140#27, 162#24, and 164#2 were subcloned into expression cassettes for the TCR-α and -β chains, which were

provided by Diane Mathis (Harvard University, Cambridge, Massachusetts, USA) (50), following appropriate treatment with restriction enzymes. The nucleotide sequences of the restriction enzyme sites *Xho*I and *Kpn*I, which were originally contained in the TCR genes and used for subcloning and linearization before transfection, were altered using a QuikChange Multi Site-Directed Mutagenesis Kit (Stratagene), preserving the amino acid sequence.

*Retroviral vector for Dsg3-reactive TCR expression.* Complementary DNAs for the TCR-α and -β chains (Supplemental Figures 1–6) were isolated from the Dsg3-reactive T cell clones 140#27, 162#24, and 164#2 and inserted into the retroviral vector pMXs (51). The retroviral vector pMXs-IG harbors the sequence encoding GFP after the internal ribosomal entry sequence (IRES), and mock retroviral vector pMXs were used as negative controls.

*Retroviral transduction.* A packaging cell line, PLAT-E, was cultured in DMEM supplemented with 10% FCS, 2 mM L-glutamine, 1 mM pyruvate, 50 U/ml penicillin, 50 μg/ml streptomycin, 0.05 mM 2-ME, 1 μg/ml puromycin, and 10 μg/ml blasticidin. Retroviral vectors were transfected into packaging cell line PLAT-E cells and the supernatant was collected, as described previously (51). $CD4^+$ T cells were enriched from splenocytes of C57BL/6 mice by positive selection using the MACS cell separation system (Miltenyi Biotec) and then cultured in 24-well plates ($10^6$ cells/well) in complete medium (RPMI 1640 containing 10% FCS, 2 mM L-glutamine, 1 mM pyruvate, 50 U/ml penicillin, 50 μg/ml streptomycin, and 0.05 mM 2-ME) supplemented with 100 U/ml hIL-2 and 2.5 μg/ml Con A at 37°C for 24 hours. In some experiments, *Ifng*$^{-/-}$ and *Il17a*$^{-/-}$ mice were used as the source of $CD4^+$ T cells. The cells remaining after $CD4^+$ T cell enrichment were irradiated (30 Gy) and used for coculture with $CD4^+$ T cells as feeder cells. The activated $CD4^+$ T cells were resuspended in retroviral supernatant and centrifuged (1400 *g*, 1 hour, 30°C). After incubation at 37°C for 4 hours, the retroviral supernatant was removed, and the cells were cultured in complete medium supplemented with 100 U/ml hIL-2 at 37°C for 44 hours.

*Generation of Dsg3-reactive TCR transgenic mice.* Linearized transgenes of the TCR-α and -β chains for the T cell clone 140#27 were injected into fertilized oocytes of C57BL/6J ($H\text{-}2^b$) mice to generate TCR transgenic mice, C57BL/6J-Tg(Dsg3TCR140), which were maintained by mating with C57BL/6J mice. The line C57BL/6J-Tg(Dsg3TCR140)1 was referred to as Dsg3H1, and female Dsg3H1 mice were used in this study. Similarly, another TCR transgenic mouse, C57BL/6J-Tg(Dsg3TCR164)3, was generated by using transgenes of the TCR-α and -β chains for T cell clones, 164#2, and referred to as Dsg3L3 mice.

*Peptide.* We purchased 111 overlapping 15-mer peptides covering EC1 to EC3 of the Dsg3 extracellular domain (aa 1–394) from Sigma-Aldrich.

*In vitro reconstitution of Dsg3-reactive TCR.* The T cell hybridoma TG40-CD4 (52, 53) (provided by Takashi Saito, Riken Research Center for Allergy and Immunology, Yokohama, Japan) loses intrinsic TCR expression and expresses mouse CD4, which was retrovirally introduced. Then, 10 μg of linearized vectors for TCR-α and -β chain expression in addition to pSV2-hph (ATCC) containing the hygromycin-resistance gene were introduced into TG40-CD4 electrically (280 V, 0.975 μF). Stable transfectants were selected by using hygromycin after electroporation. The expression of transduced vectors was confirmed by flow cytometry, detecting coexpression of TCR-β and CD3, which is expressed as a complex with both the TCR-α and -β chains. Stable transfectants were sorted by a MACS cell isolation system using anti-TCRβ6 Ab-PE or anti-TCRβ8 Ab-PE (BD) in combination with anti–PE Ab microbeads (Miltenyi Biotech).

*Reactivity of T cells and T cell hybridomas against Dsg3 peptides.* A single-cell suspension of $4 \times 10^4$ cells was prepared from the spleens of TCR transgenic mice and cultured with $1 \times 10^5$ 40 Gy–irradiated splenocytes and 10 μg/ml peptide in a 96-well round-bottom plate, and Dsg3-specific T cell proliferation was measured by $^3$H-thymidine uptake, as described previously (54). $2 \times 10^4$ T cell hybridoma cells were cultured with $1 \times 10^6$ 40 Gy–irradiated splenocytes and the peptide at the indicated concentration in 96-well flat-bottom plates for 24 hours. Subsequently, the culture supernatant was subjected to IL-2 ELISA (BD). Some of the experiments were performed in combination with anti-MHC class II mAb (M5/114) or isotype-matched rat mAb (BD).

*Flow cytometry.* A single-cell suspension of thymus, spleen, or lymph nodes from mice was stained appropriately using CD4-FITC, CD25-FITC, CD44-FITC, IL-17A–FITC, IFN-γ–FITC, TCR-β–PE, TCR-Vβ6–PE, CD4-PerCP-Cy5.5, CD8-PerCP-Cy5.5, 7-AAD, CD25-APC, CD24-APC, IL-4–APC, Foxp3-APC, CD45-APC/Cy7, CD4-PE/Cy7, CD62L-biotin, and CD229.1-biotin in combination with streptavidin-APC. The reagents in the anti-mouse/rat Foxp3 Staining Set (eBioscience) were used for intracellular staining following treatment with PMA, ionomycin, and brefeldin A (Sigma-Aldrich). For intracellular staining, 7-AAD was washed with PBS twice before fixation.

*Generation of bone marrow chimeric mice.* CD3-depleted BM cells from Dsg3H1 mice were prepared using CD3 microbeads (Miltenyi Biotech) and transferred intravenously into 7 Gy–irradiated 129/Sv mice or 129/Sv *Dsg3*$^{-/-}$ mice. Two months later, the recipient mice were used for further experiments.

*Adoptive transfer.* *Dsg3*$^{-/-}$ B cells were prepared from *Dsg3*$^{-/-}$ mice, as described previously (7). $CD4^+V\beta6^+$ T cells were prepared from the spleens and LNs of Dsg3H1 or Dsg3L3 mice by depleting $B220^+$ and $CD8^+$ cells, followed by positive selection of $V\beta6^+$ cells using the MACS cell separation system (Miltenyi Biotech). Then $5 \times 10^6$ *Dsg3*$^{-/-}$ B cells and $2.5 \times 10^6$ $CD4^+V\beta6^+$ T cells were transferred into *Rag2*$^{-/-}$ mice intravenously. In some experiments, retrovirally transduced $CD4^+$ T cells were transferred into *Rag2*$^{-/-}$ mice in combination with or without *Dsg3*$^{-/-}$ B cells. For CFSE labeling, $CD4^+$ T cells were isolated by depleting $B220^+$, $CD8^+$, $Gr\text{-}1^+$, and $CD11b^+$ cells from splenocytes and LN cells of Dsg3H1 mice by MACS and labeled with CFSE (Molecular Probes) before adoptive transfer, as described previously (7). Naive $Ly9.1^-CD4^+$ T cells derived from Dsg3H1→WT and Dsg3H1→*Dsg3*$^{-/-}$ mice, referred to as Dsg3H1→WT and Dsg3H1→*Dsg3*$^{-/-}$ $CD4^+$ T cells, respectively, were prepared by depleting $Ly9.1^+$, $B220^+$, $CD8^+$, $Gr\text{-}1^+$, $CD11b^+$, $DX5^+$, and $CD44^+$ cells from splenocytes and LN cells with magnetic beads, and $3\text{–}15 \times 10^5$ T cells were transferred with *Dsg3*$^{-/-}$ B cells into *Rag2*$^{-/-}$ mice.

*Anti-Dsg3 Ab detection.* Anti-Dsg3 IgG Ab was quantified by ELISA and detected by living cell staining, as described previously (49).

*Immunoprecipitation-immunoblotting.* Immunoprecipitation-immunoblotting was performed according to the previous report with some modification, in which we used primary mouse keratinocytes as a source of substrate (55).

*Histological analysis.* Formalin-fixed tissue was stained with H&E, and observed with an inverted TE2000-U microscope (Nikon). For immunofluorescent staining, 10-μm cryosections of the palate were fixed with acetone, and then stained with anti-mouse IgG Ab Alexa Fluor 488 (Molecular Probes), anti-TCRβ Ab-PE, and TOTO3 (Molecular Probes). Sections were observed under a confocal laser fluorescence FV1000 microscope (Olympus).

*Statistics.* Statistical analyses were made using the Mann-Whitney *U* test. Data represent mean ± SEM. $P < 0.05$ was considered significant.

## Acknowledgments

We thank Diane Mathis (Harvard University) for the gift of cassette vectors for TCR-α and -β chain expression, Takashi Saito (Riken Research Center for Allergy and Immunology, Yokohama, Japan) for the TG40-CD4 T cell hybridoma cell line, Toshio Kitamura (Institute of Medical Science, University of Tokyo) for the pMXs retroviral vector and PLAT-E packaging cell line, H. Itoh for providing excellent animal care, and M. Suzuki for preparing the cryosections. This work was supported by Grants-in-Aid for Scientific Research from the Ministry of Education, Culture, Sports, Science and Technology of Japan; Health and Labor Sciences Research Grants for Research on Measures for Intractable Diseases from the Ministry of Health, Labor and Welfare of Japan;

the Uehara Memorial Foundation; and Keio Gijuku Academic Development Funds.
Received for publication February 1, 2011, and accepted in revised form June 11, 2011.

Address correspondence to: Masayuki Amagai, Department of Dermatology, Keio University School of Medicine, 35 Shinanomachi, Shinjuku-ku, Tokyo 160-8582, Japan. Phone: 81.3.5363.3822; Fax: 81.3.3351.6880; E-mail: amagai@a7.keio.jp.

1. Amagai M, Klaus-Kovtun V, Stanley JR. Autoantibodies against a novel epithelial cadherin in pemphigus vulgaris, a disease of cell adhesion. *Cell.* 1991;67(5):869–877.
2. Amagai M, Hashimoto T, Shimizu N, Nishikawa T. Absorption of pathogenic autoantibodies by the extracellular domain of pemphigus vulgaris antigen (Dsg3) produced by baculovirus. *J Clin Invest.* 1994;94(1):59–67.
3. Tsunoda K, et al. Induction of pemphigus phenotype by a mouse monoclonal antibody against the amino-terminal adhesive interface of desmoglein 3. *J Immunol.* 2003;170(4):2170–2178.
4. Amagai M. Autoimmune and infectious skin diseases that target desmogleins. *Proc Jpn Acad Ser B Phys Biol Sci.* 2010;86(5):524–537.
5. Raff MC. Role of thymus-derived lymphocytes in the secondary humoral immune response in mice. *Nature.* 1970;226(5252):1257–1258.
6. Garside P, Ingulli E, Merica RR, Johnson JG, Noelle RJ, Jenkins MK. Visualization of specific B and T lymphocyte interactions in the lymph node. *Science.* 1998;281(5373):96–99.
7. Takahashi H, Amagai M, Nishikawa T, Fujii Y, Kawakami Y, Kuwana M. Novel system evaluating in vivo pathogenicity of desmoglein 3-reactive T cell clones using murine pemphigus vulgaris. *J Immunol.* 2008;181(2):1526–1535.
8. Takahashi H, Kuwana M, Amagai M. A single helper T cell clone is sufficient to commit polyclonal naive B cells to produce pathogenic IgG in experimental pemphigus vulgaris. *J Immunol.* 2009; 182(3):1740–1745.
9. Anhalt GJ, et al. Paraneoplastic pemphigus. An autoimmune mucocutaneous disease associated with neoplasia. *N Engl J Med.* 1990;323(25):1729–1735.
10. Hoffman MA, Qiao X, Anhalt GJ. CD8+ T lymphocytes in bronchiolitis obliterans, paraneoplastic pemphigus, and solitary Castleman's disease. *N Engl J Med.* 2003;349(4):407–408.
11. Nikolskaia OV, Nousari CH, Anhalt GJ. Paraneoplastic pemphigus in association with Castleman's disease. *Br J Dermatol.* 2003;149(6):1143–1151.
12. Amagai M, Nishikawa T, Nousari HC, Anhalt GJ, Hashimoto T. Antibodies against desmoglein 3 (pemphigus vulgaris antigen) are present in sera from patients with paraneoplastic pemphigus and cause acantholysis in vivo in neonatal mice. *J Clin Invest.* 1998;102(4):775–782.
13. Anhalt GJ. Paraneoplastic pemphigus. *Adv Dermatol.* 1997;12:77–96.
14. Sontheimer RD. Lichenoid tissue reaction/interface dermatitis: clinical and histological perspectives. *J Invest Dermatol.* 2009;129(5):1088–1099.
15. Matsuoka LY. Graft versus host disease. *J Am Acad Dermatol.* 1981;5(5):595–599.
16. Pereira FA, Mudgil AV, Rosmarin DM. Toxic epidermal necrolysis. *J Am Acad Dermatol.* 2007; 56(2):181–200.
17. Oliver GF, Winkelmann RK, Muller SA. Lichenoid dermatitis: a clinicopathologic and immunopathologic review of sixty-two cases. *J Am Acad Dermatol.* 1989;21(2 pt 1):284–292.
18. Rudensky A, Preston-Hurlburt P, Hong SC, Barlow A, Janeway CA Jr. Sequence analysis of peptides bound to MHC class II molecules. *Nature.* 1991;353(6345):622–627.
19. Chicz RM, Urban RG, Gorga JC, Vignali DA, Lane WS, Strominger JL. Specificity and promiscuity among naturally processed peptides bound to HLA-DR alleles. *J Exp Med.* 1993;178(1):27–47.
20. Hata T, et al. Transgenic rescue of desmoglein 3 null mice with desmoglein 1 to develop a syngeneic mouse model for pemphigus vulgaris. *J Dermatol Sci.* 2011;63(1):33–39.
21. Weedon D. *Weedon's Skin Pathology.* Amsterdam, The Netherlands: Churchill Livingstone; 2009.
22. Bolognia JL, Jorizzo JL, Rapini RP. *Dermatology.* 2nd ed. Amsterdam, The Netherlands: Elsevier, Mosby, Saunders; 2008.
23. Akasu R, From L, Kahn HJ. Lymphocyte and macrophage subsets in active and inactive lesions of lichen planus. *Am J Dermatopathol.* 1993;15(3):217–223.
24. Freedberg IM, et al. *Fitzpatrick's Dermatology in General Medicine.* New York, New York, USA: McGraw-Hill Publishing; 1999.
25. Burns T, Breathnach S, Cox N, Griffiths C. *Rook's Textbook of Dermatology.* Oxford, United Kingdom: Wiley-Blackwell; 2005.
26. Shiohara T, Moriya N, Tsuchiya K, Nagashima M, Narimatsu H. Lichenoid tissue reaction induced by local transfer of Ia-reactive T-cell clones. *J Invest Dermatol.* 1986;87(1):33–38.
27. Lafaille JJ, Nagashima K, Katsuki M, Tonegawa S. High incidence of spontaneous autoimmune encephalomyelitis in immunodeficient anti-myelin basic protein T cell receptor transgenic mice. *Cell.* 1994;78(3):399–408.
28. Oyama N, et al. Autoantibodies to extracellular matrix protein 1 in lichen sclerosus. *Lancet.* 2003; 362(9378):118–123.
29. Baldo M, Bailey A, Bhogal B, Groves RW, Ogg G, Wojnarowska F. T cells reactive with the NC16A domain of BP180 are present in vulval lichen sclerosus and lichen planus. *J Eur Acad Dermatol Venereol.* 2010;24(2):186–190.
30. Sugerman PB, Satterwhite K, Bigby M. Autocytotoxic T-cell clones in lichen planus. *Br J Dermatol.* 2000;142(3):449–456.
31. McInnes IB, Schett G. Cytokines in the pathogenesis of rheumatoid arthritis. *Nat Rev Immunol.* 2007;7(6):429–442.
32. Bettelli E, Oukka M, Kuchroo VK. T(H)-17 cells in the circle of immunity and autoimmunity. *Nat Immunol.* 2007;8(4):345–350.
33. Lubberts E, et al. Treatment with a neutralizing anti-murine interleukin-17 antibody after the onset of collagen-induced arthritis reduces joint inflammation, cartilage destruction, and bone erosion. *Arthritis Rheum.* 2004;50(2):650–659.
34. Nakae S, Nambu A, Sudo K, Iwakura Y. Suppression of immune induction of collagen-induced arthritis in IL-17-deficient mice. *J Immunol.* 2003; 171(11):6173–6177.
35. Murphy CA, et al. Divergent pro- and antiinflammatory roles for IL-23 and IL-12 in joint autoimmune inflammation. *J Exp Med.* 2003;198(12):1951–1957.
36. Bending D, et al. Highly purified Th17 cells from BDC2.5NOD mice convert into Th1-like cells in NOD/SCID recipient mice. *J Clin Invest.* 2009; 119(3):565–572.
37. Wang B, et al. Interferon-gamma impacts at multiple points during the progression of autoimmune diabetes. *Proc Natl Acad Sci U S A.* 1997; 94(25):13844–13849.
38. Campbell IL, Kay TW, Oxbrow L, Harrison LC. Essential role for interferon-gamma and interleukin-6 in autoimmune insulin-dependent diabetes in NOD/Wehi mice. *J Clin Invest.* 1991;87(2):739–742.
39. Langrish CL, et al. IL-23 drives a pathogenic T cell population that induces autoimmune inflammation. *J Exp Med.* 2005;201(2):233–240.
40. O'Connor RA, et al. Cutting edge: Th1 cells facilitate the entry of Th17 cells to the central nervous system during experimental autoimmune encephalomyelitis. *J Immunol.* 2008;181(6):3750–3754.
41. Jager A, Dardalhon V, Sobel RA, Bettelli E, Kuchroo VK. Th1, Th17, and Th9 effector cells induce experimental autoimmune encephalomyelitis with different pathological phenotypes. *J Immunol.* 2009;183(11):7169–7177.
42. Nakae S, et al. Antigen-specific T cell sensitization is impaired in IL-17-deficient mice, causing suppression of allergic cellular and humoral responses. *Immunity.* 2002;17(3):375–387.
43. Amrani A, Verdaguer J, Thiessen S, Bou S, Santamaria P. IL-1alpha, IL-1beta, and IFN-gamma mark beta cells for Fas-dependent destruction by diabetogenic CD4(+) T lymphocytes. *J Clin Invest.* 2000;105(4):459–468.
44. Wilson CB, Rowell E, Sekimata M. Epigenetic control of T-helper-cell differentiation. *Nat Rev Immunol.* 2009;9(2):91–105.
45. Trinchieri G, Pflanz S, Kastelein RA. The IL-12 family of heterodimeric cytokines: new players in the regulation of T cell responses. *Immunity.* 2003;19(5):641–644.
46. Azukizawa H, et al. Induction of T-cell-mediated skin disease specific for antigen transgenically expressed in keratinocytes. *Eur J Immunol.* 2003; 33(7):1879–1888.
47. Shibaki A, Sato A, Vogel JC, Miyagawa F, Katz SI. Induction of GVHD-like skin disease by passively transferred CD8(+) T-cell receptor transgenic T cells into keratin 14-ovalbumin transgenic mice. *J Invest Dermatol.* 2004;123(1):109–115.
48. Wada N, et al. Aire-dependent thymic expression of desmoglein 3, the autoantigen in pemphigus vulgaris, and its role in T-cell tolerance. *J Invest Dermatol.* 2011;131(2):410–417.
49. Amagai M, Tsunoda K, Suzuki H, Nishifuji K, Koyasu S, Nishikawa T. Use of autoantigen-knockout mice in developing an active autoimmune disease model for pemphigus. *J Clin Invest.* 2000;105(5):625–631.
50. Kouskoff V, Signorelli K, Benoist C, Mathis D. Cassette vectors directing expression of T cell receptor genes in transgenic mice. *J Immunol Methods.* 1995;180(2):273–280.
51. Kitamura T, et al. Retrovirus-mediated gene transfer and expression cloning: powerful tools in functional genomics. *Exp Hematol.* 2003;31(11):1007–1014.
52. Sussman JJ, Saito T, Shevach EM, Germain RN, Ashwell JD. Thy-1- and Ly-6-mediated lymphokine production and growth inhibition of a T cell hybridoma require co-expression of the T cell antigen receptor complex. *J Immunol.* 1988; 140(8):2520–2526.
53. Zumla A, et al. Co-expression of human T cell receptor chains with mouse CD3 on the cell surface of a mouse T cell hybridoma. *J Immunol Methods.* 1992;149(1):69–76.
54. Kuwana M, Medsger TA Jr, Wright TM. T cell proliferative response induced by DNA topoisomerase I in patients with systemic sclerosis and healthy donors. *J Clin Invest.* 1995;96(1):586–596.
55. Hashimoto T, et al. Novel non-radioisotope immunoprecipitation studies indicate involvement of pemphigus vulgaris antigen in paraneoplastic pemphigus. *J Dermatol Sci.* 1998;17(2):132–139.

Jpn J Ophthalmol (2011) 55:405–410
DOI 10.1007/s10384-011-0030-6

LABORATORY INVESTIGATION

# Expression of interleukin-4 receptor α in human corneal epithelial cells

**Mayumi Ueta · Chie Sotozono · Shigeru Kinoshita**

Received: 18 May 2010 / Accepted: 12 January 2011 / Published online: 27 May 2011


**Abstract**
*Purpose* We previously reported that human conjunctival epithelial cells expressed functioning interleukin-4 receptor α (IL-4Rα). In this study, we investigated whether human corneal epithelial cells also express functioning IL-4Rα.
*Methods* The presence of IL-4Rα mRNA and protein in human corneal epithelium was examined by reverse-transcriptase polymerase chain reaction (RT-PCR) and immunohistology, respectively. The cell surface expression of IL-4Rα and the transcripts upregulated upon IL-4Rα ligand (IL-4 or IL-13) stimulation were examined by flow cytometry and quantitative RT-PCR, respectively, using immortalized human corneal-limbal epithelial (HCLE) cells.
*Results* The mRNA and protein of IL-4Rα were detected in human corneal epithelium. Flow cytometry analysis showed the cell surface expression of IL-4Rα protein. Quantitative RT-PCR assay of HCLE cells showed the upregulation of the transcripts tumor necrosis factor alpha-induced protein 6 (TNFAIP6), RAS guanyl-releasing protein 1 (RASGRP1), carbonic anhydrase II (CA2), cytokine-inducible SH2-containing protein (CISH), hyaluronan synthase 3 (HAS3), calpain 14 (CAPN14), endothelin receptor type A (EDNRA), cathepsin C (CTSC), and lecithin retinol acyltransferase (LRAT) as well as human conjunctival epithelial cells.
*Conclusion* Human corneal epithelial cells expressed functioning IL-4Rα, and stimulation of its ligands, IL-4 and IL-13, could induce the expression of various genes, e.g., antiinflammatory molecule genes such as *TNFAIP6* and *CISH* and cellular differentiation and proliferation-related molecule genes such as *RASGRP1*, *HAS3*, *EDNRA*, and *LRAT*.

**Keywords** Interleukin-4 receptor α (IL-4Rα) · Human corneal epithelial cells · Interleukin-4 (IL-4) · Interleukin-13 (IL-13)

## Introduction

We previously reported that human conjunctival epithelial cells expressed functioning interleukin-4 receptor α (IL-4Rα) and that stimulation of IL-4 could induce the expression of various genes such as tumor necrosis factor alpha-induced protein 6 (*TNFAIP6*), RAS guanyl-releasing protein 1 (*RASGRP1*), carbonic anhydrase II (*CA2*), cathepsin C (*CTSC*), hyaluronan synthase 3 (*HAS3*), calpain 14 (*CAPN14*), endothelin receptor type A (*EDNRA*), cytokine-inducible SH2-containing protein (*CISH*), and lecithin retinol acyltransferase (*LRAT*) [1]. Comprehensive gene expression analysis using GeneChip revealed their transcripts to be upregulated by more than fourfold in human conjunctival epithelial cells upon IL4 stimulation [1].

Interleukin-4 receptor α, a component of the receptor of IL-4 and IL-13, is essential for both IL-4 and IL-13 signaling. The type-I IL-4 receptor is composed of two subunits: an α subunit (IL-4Rα) that binds IL-4 and transduces its growth-promoting and transcription-activating functions,

M. Ueta (✉) · C. Sotozono · S. Kinoshita
Department of Ophthalmology, Kyoto Prefectural University of Medicine, 465 Kajii-cho, Hirokoji-agaru, Kawaramachi-dori, Kamigyo-ku, Kyoto 602-0841, Japan
e-mail: mueta@koto.kpu-m.ac.jp

M. Ueta
Research Center for Inflammation and Regenerative Medicine, Faculty of Life and Medical Sciences, Doshisha University, Kyoto, Japan

and a γc subunit, common to several cytokine receptors, that amplifies IL-4Rα signaling. The IL-13 receptor is composed of the IL-4Rα chain and the IL-13Rα1 chain.

We previously reported that IL-4Rα is also a candidate gene for Stevens-Johnson syndrome (SJS)/toxic epidermal necrolysis (TEN) with ocular complications [2, 3]. Interleukin-4 receptor α is also a candidate gene for allergic diseases such as atopy and asthma, which are biologically linked to T-helper type 2 (Th2) cytokine-driven inflammatory mechanisms [4, 5]. We have also reported that ocular surface epithelial cells regulated ocular surface inflammation [6–18]. Thus, we focused on ocular surface epithelial cells and examined the function of IL-4Rα in not only conjunctival epithelium [1], but also corneal epithelium.

Although many reports regarding IL-4Rα expression and function in human corneal fibroblasts have been published [19–21], to the best of our knowledge, there are no reports of IL-4Rα expression and function in human corneal epithelial cells. Thus, in this study we examined the expression and function of IL-4Rα in human corneal epithelium.

## Materials and methods

### Human corneal epithelial cells

This study was approved by the Institutional Review Board of Kyoto Prefectural University of Medicine, Kyoto, Japan. All experimental procedures were conducted in accordance with the tenets set forth in the Declaration of Helsinki. The purpose of the research and the experimental protocols were explained in detail to all patients, and informed consent was obtained from them prior to their participation in the study.

For the reverse transcription polymerase chain reaction (RT-PCR), human corneal epithelial cells were obtained from two corneal grafts after corneal transplantations for bullous keratopathy and from one corneal tissue supplied by the Northwest Lions Eye Bank (Seattle, WA). For immunohistological analysis, human corneal tissue sections were prepared from corneal grafts after corneal transplantations for bullous keratopathy of early stage Fuchs' corneal dystrophy. Immortalized human corneal-limbal epithelial (HCLE) cells were a gift from Dr. Ilene K. Gipson and cultured in low-calcium defined keratinocyte-SFM medium (dk-SFM; Invitrogen, Carlsbad, CA) with defined growth-promoting additives, including insulin, epidermal growth factor, and fibroblast growth factor, and 1% antibiotic-antimycotic solution. After reaching 80% confluence, they were used in the subsequent procedures.

### RT-PCR

Human corneal epithelium was analyzed for IL-4R mRNA expression as described in our previous study [1]. Briefly, total RNA was isolated from human corneal epithelium and human peripheral mononuclear cells using the RNeasy kit (Qiagen, Valencia, CA) according to the manufacturer's instructions. For the RT reaction, we used the SuperScript Preamplification kit (Invitrogen). Polymerase chain reaction amplification was performed with DNA polymerase (ExTaq; Takara, Shiga, Japan); the conditions were 38 cycles at 95°C for 1 min, followed by 95°C for 30 s, 55°C for 30 s, and 72°C for 1 min, with final extension at 72°C for 2 min on a commercial PCR machine (GeneAmp; Applied Biosystems, Foster City, CA). The specific primers for IL4R and glyceraldehyde-3-phosphate dehydrogenase (GAPDH) have been previously reported [1]. RNA integrity was assessed electrophoretically in ethidium bromide-stained 1.5% agarose gels.

### Immunohistological study of IL-4Rα in human corneal sections

Serial sections of human corneal tissue were prepared from corneal grafts after corneal transplantations for bullous keratopathy of early stage Fuchs' corneal dystrophy. The sections were fixed for 30 min with methanol, incubated overnight in a moist chamber at 4°C with mouse anti-human IL-4Rα monoclonal antibody (mAb; R&D Systems, Minneapolis, MN), or isotype control mouse IgG2a (DakoCytomation, Kyoto, Japan), and then washed in phosphate-buffered saline (PBS). Alexa Fluor 488 goat anti-mouse IgG (H + L) (Molecular Probes, Eugene, OR) was applied for 1 h at room temperature, and the slides were then washed again in PBS, and antifade mounting medium containing propidium iodide (PI) (Vectashield; Vector Laboratories, Burlingame, CA) was applied [1].

### Flow cytometric analysis

The HCLE cells were analyzed for cell surface expression of IL-4Rα by flow cytometry as previously described [1]. Briefly, HCLE cells were treated with 0.02% ethylenediaminetetraacetic acid (EDTA) and then incubated with mAb (R&D Systems) or isotype control mouse IgG2a (DakoCytomation) for 30 min at 4°C. Alexa Fluor 488 goat anti-mouse IgG (H + L) (molecular probes) was used as the secondary antibody. Stained cells were analyzed with a FACS Calibur (Becton, Dickinson and Co., San Jose, CA). The data were analyzed using Cellquest software (Becton, Dickinson and Co.).

### Quantitative RT-PCR

For quantitative RT-PCR, HCLE cells were exposed to 10 ng/ml of IL-4 or IL-13 for 6 h. Quantitative RT-PCR was performed on an ABI Prism 7700 Sequence Detection System (Applied Biosystems) according to previously described procedures [1]. The primers and probes were purchased from Applied Biosystems. The quantification data were normalized to the expression of the housekeeping gene GAPDH.

### Data analysis

Data were expressed as the mean ± standard error of the mean (SEM) and evaluated by the *t* test using the Excel program.

## Results

### Expression of IL4Rα in human corneal epithelium

Interleukin-4 receptor α-specific mRNA expression was present in human corneal epithelium (Fig. 1a). This finding demonstrates that the *IL-4Rα* gene is constitutively expressed in human corneal epithelium. The corneal tissues were subjected to immunohistochemical study to determine the presence and localization of IL-4Rα expression in stratified corneal epithelium. Interleukin-4Rα protein was consistently and abundantly expressed and located in cells from the basal to the superficial layer of the human corneal epithelium (Fig. 1b). Flow cytometry analysis showed that IL-4Rα protein was also expressed at the cell surface of the HCLE cells at levels comparable to those of human conjunctival epithelial cells (Fig. 1c).

### Upregulation of transcripts upon IL-4 and IL-13 stimulation

We previously reported that 9 transcripts (TNFAIP6, RASGRP1, CA2, CTSC, HAS3, CAPN14, EDNRA, CISH, and LRAT) were upregulated upon IL-4 stimulation in human conjunctival epithelial cells [1]. We here examined whether human corneal epithelial cells also upregulated these 9 transcripts upon IL-4 or IL-13 stimulation by quantitative RT-PCR assay. Our results showed that both IL-4 and IL-13 could upregulate these 9 transcripts in human corneal epithelial cells, although the upregulation by IL-4 stimulation was stronger than that by IL-13 stimulation (Fig. 2). Moreover, we confirmed that neither IL-4 nor IL-13 stimulation for 6 h promoted cell proliferation in HCLE.

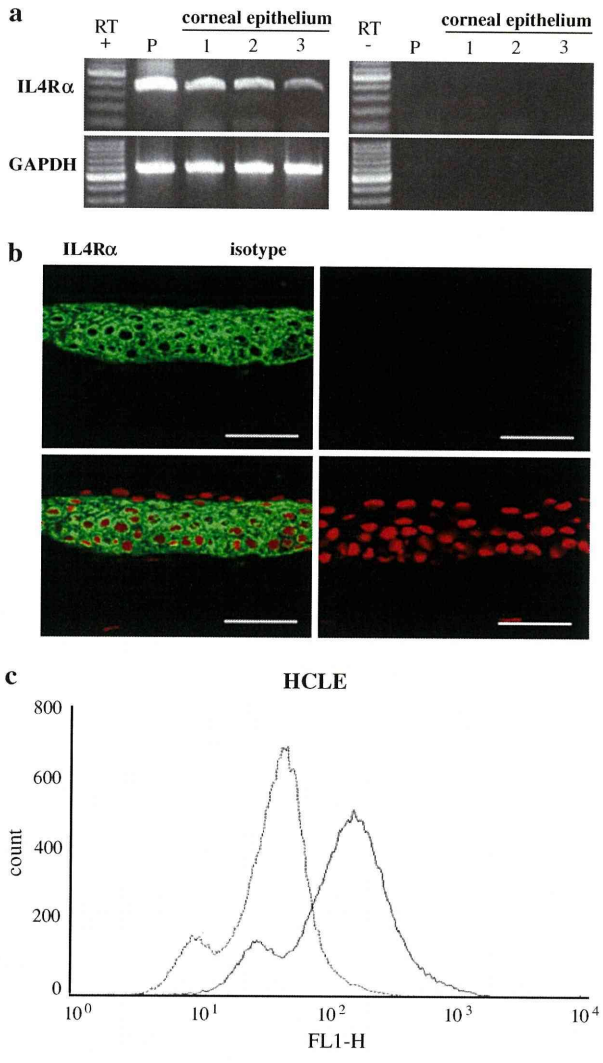


**Fig. 1** **a** Reverse-transcriptase polymerase chain reaction (RT-PCR) analyses of the expression of interleukin-4 receptor α (IL4Rα)-specific mRNA in human corneal epithelium. As a positive control, mRNA isolated from human peripheral blood mononuclear cells was subjected to RT-PCR (*left column*). *RT−* indicates that data were obtained without reverse transcription (controls). **b** Immunohistological analysis of IL4Rα in human corneal epithelium. Bound antibodies were visualized by Alexa Fluor 488 goat anti-mouse IgG−, and nuclei, by propidium iodide (PI) staining. Propidium iodide is absent in the upper column and present in the lower column. Each *bar* represents a length of 50 μm. **c** Flow cytometry analysis of the cell surface expression of IL4Rα in HCLE cells. The histogram data are representative of 3 separate experiments (*solid line*, IL4Rα antibody; *dotted line*, isotype control)

## Discussion

Our results showed that the mRNA and protein of IL-4Rα were detected in human corneal epithelium. Interleukin-4 and IL-13, which are ligands of IL-4Rα, induced the upregulation of 9 transcripts—TNFAIP6, RASGRP1, CA2,